Final Project Report
Research Project 1037

Development of a Simplified Methodology to Incorporate Radiant Heaters Over 300°F into Thermal Comfort Calculations

Prepared for:
The American Society
of Heating, Refrigerating, and Air-Conditioning Engineers

Prepared by:
Kirby S. Chapman, Ph.D.
Wen Wang, Research Assistant
National Gas Machinery Laboratory
Kansas State University
245 Levee Drive
Manhattan, Kansas 66502

January, 2003

Table of Contents

1.0 Introduction

High-temperature radiant heaters – those with a surface temperature greater than 300°F – typically are applied in large, open, and occupied spaces, such as warehouses and aircraft hangers. These heaters provide an efficient means of delivering thermal comfort to specific work stations without having to condition the entire occupied space. Highly efficient thermal comfort can be delivered because radiant heaters focus thermal energy, and therefore thermal comfort, directly on the occupants, rather than controlling room temperature as do other heating systems.

The objective of this research study was to develop a simplified thermal comfort methodology that reliably calculates the thermal comfort effect, as expressed as the operative temperature, of high-temperature radiant heaters. The developed methodology would be an add-on module to the already-existing Discrete-Ordinates Radiation Solver used in the Building Comfort Analysis Program (BCAP), which was developed under ASHRAE project RP-657 (Chapman, 1994).

This research report contains: 1) a study of the types of high-temperature radiant heaters and the mathematical heat transfer characteristics of each; 2) an examination of radiation models; 3) a review of thermal comfort and radiant heat transfer measures; 4) an explanation of the developed model; and 5) several case studies where the model is applied. The developed method can be used as a design tool for sizing and placing high-temperature radiant systems, possibly in combination with other heating systems as it encompasses a wide range of building materials and operating conditions.

2.0 High-Temperature Radiant Heaters

Over the years, high temperature radiant heaters have been utilized in many industrial applications as well as residential space heating. As energy efficiency is becoming more important, engineers have sought for a better design and allocation of these heaters. This section explains the types of high-temperature gas-fired radiant heaters and the heat transfer implications of these heaters. To determine the energy available from each heater type, various mathematical models are discussed. In addition, design parameters to size and locate heaters for optimal operations are considered. After the energy available from each type of high-temperature radiant heater is determined, then the radiant transfer to the occupants is examined.

The literature review was conducted utilizing the resources of the Gas Research Institute, the library at Kansas State University, *ASHRAE Transactions*, and the interlibrary loan through Kansas State University library.

2.1 Types of High-Temperature Radiant Heaters: Direct and Indirect

For residential use, a direct radiant heater typically consists of a porous ceramic or metal screen as a flat combustion surface, which is classified by the American Society of Heating Refrigerating and Air-Conditioning Engineers (ASHRAE) as a surface combustion heater (ASHRAE, 1996). Manufacturers' standards often refer to these heaters as high intensity radiant heaters because of the high temperature at the burning surface, which can reach approximately 900°C under normal operating conditions (ASHRAE, 1996, Solaronics, 1994a/b). In these types of heaters, the gas and air are pre-mixed, and the combustion takes place on the burner face. Figure 1 illustrates a typical gas-fired surface combustion heater with reflector. Sufficient room ventilation is necessary in order to use these heaters since the heater usually does not include ventilating system.

An indirect radiant heater, also called a low intensity radiant heater, has a tubular combustion cell. Since the combustion occurs in the tube and the heater has exhaust ventilation piping, no interaction takes place between the room air and the combustion products. The tube is

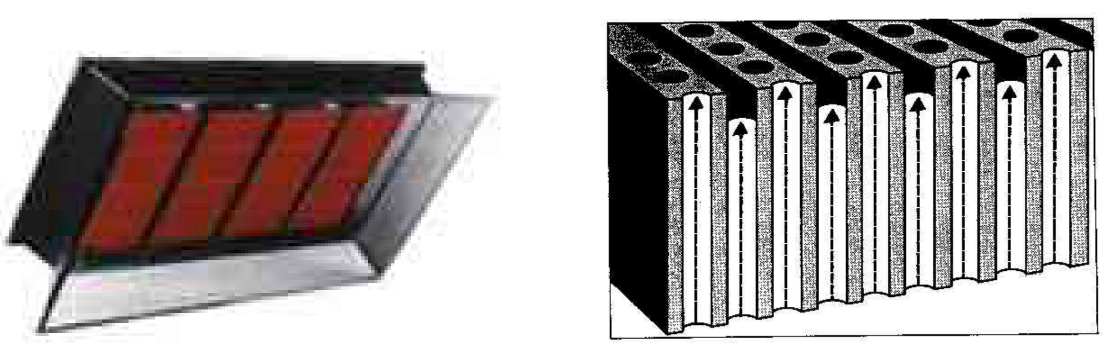

Figure 1: Gas-fired Direct Radiant Heater and its Surface Structure (Solaronics, Inc., 1994a).

made of either a heat resistant steel or ceramic, while the shape of the tube depends on the design. Various shapes include: straight-through, U-type, W-type, and blinded-end (Harder *et al.*, 1987). A straight-through radiant tube, shown in Figure 2, is the simplest; however, it suffers from relatively large longitudinal thermal expansion that reduces its service life (Chapman *et al.*, 1988). The U- and W-types, shown in Figures 3 and 4 respectively, have combustion reactant and product going through the same side of the heater. This design has successfully increased the service life over the straight-through type. Nevertheless, they have a disadvantage as far as maintenance and thermal efficiency are concerned. The blinded-end radiant tube is the optimum among these with its simple design, uniform temperature distribution, and high thermal efficiency (Chapman *et al.*, 1988). Figure 5 illustrates of the blinded-end radiant tube heater.

Figure 2: Straight-through Radiant Tube Heater (Solaronics, Inc., 1994b).

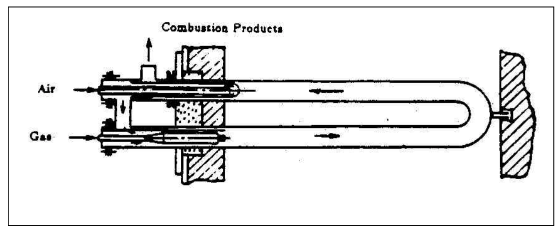

Figure 3: U-type Radiant Heater (Chapman *et al.*, 1988).

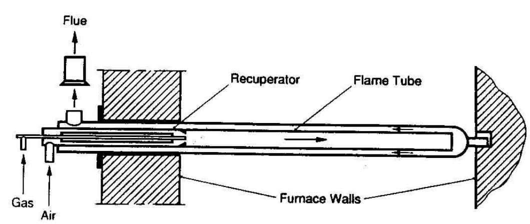

Figure 4: W-type Radiant Heater (Chapman *et al.*, 1988).

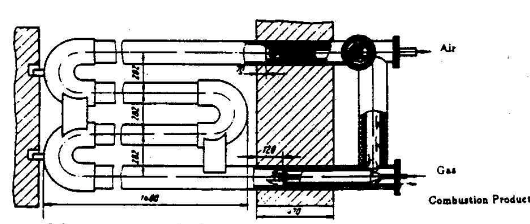

Figure 5: Blinded-end Radiant Heater (Chapman *et al.*, 1988).

2.1.1 Heat Transfer from Indirect High-Temperature Radiant Heaters

Combustion occurs inside the tubular structure of an indirect, gas-fired radiant tube heater. Specifically, a hydrocarbon gas, such as natural gas or propane, partially mixes with air and then combusts at the combustion burner inside the tubular structure. The combustion products flow into the radiant tube and then the energy released by the combustion is partially transferred to the tube (Harder *et al*., 1987). The heated tube transports the heat to the space and occupants in the room. The flow rate of the fuel mixture determines the rate of heat generation available. The parameters that are related to the optimum design of the radiant tubes include: tube wall temperature uniformity, radiant tube thermal efficiency, and tube service life (Harder *et al*., 1987).

Convection occurs due to the temperature difference between the tube surface and air in the room. A rise in temperature of the air by this convection would certainly contribute to the occupants' thermal comfort. The radiant intensity resulting from surface emission of the tube is the principal mechanism, however, by which thermal energy is delivered to the occupants. Assuming a negligible effect of moisture content of the air in question, the tube surface emits radiative energy toward all the other surfaces in all directions in the room. A typical tube heater includes a reflector located above the tube helps to focus the intensity field toward the occupants' space. This intensity field is a result of the direct radiant intensity from the tube and the reflected radiant intensity from the reflector.

2.1.2 Mathematical Model of Indirect High-Temperature Radiant Heaters

While energy transfer from a radiant tube heater to the surroundings remains the same for all types of designs, the mathematical modeling of this process depends on a heater's geometric design and operating assumptions. To understand the basic concept of the modeling scheme that is necessary to predict the energy generated by the radiant heater, consider a simple one-dimensional model for a straight-through radiant tube heater.

As for most of thermal systems, the three basic principles of modeling a radiant heater are conservation of mass, momentum, and energy. With steady-state conditions and an axially symmetric flow in the tube, these equations are (Chapman *et al*., 1988):

$$\frac{d(\rho V)}{dz} = 0 \tag{2.1}$$

$$\rho V \frac{dV}{dz} + \frac{dp}{dz} + \frac{2\tau}{r_i} = 0 \tag{2.2}$$

$$\dot{m} c_p \frac{dT_g}{dz} = h_i P_i (T_w - T_g) + \Delta h_{fuel} \frac{d\dot{m}_{fuel}}{dz} - P_i q_{rad_i} \tag{2.3}$$

where i is the inside of the tube; Δh_{fuel} is the heat of formation of the fuel; P is the perimeter; and h represents the convective heat transfer coefficient. The shear stress, τ, due to friction in the momentum equation can be expressed as (Chapman et al., 1988):

$$\tau = \frac{\rho V^2}{8} f \tag{2.4}$$

where f is the friction factor of the tube. The convective heat transfer coefficient in equation (2.3) and the friction factor in equation (2.4) depend on whether the flow is laminar or turbulent. Ideal gas behavior is assumed for the fuel-air mixture, and the co-existence of air, fuel, and combustion products also is assumed at any axial location in the tube. In order to incorporate different compositions of each constituent at an arbitrary location, the notion of a fuel burn-up ratio is employed, which was introduced by Lisenko *et al.* (1986). The functional expression for the fuel burn-up ratio is:

$$k = 1 - \exp(-4 \frac{z}{D} \mathrm{Re}_D^{-0.3}) \tag{2.5}$$

where D is the inner diameter of the tube. Lisenko *et al.* (1986) developed this correlation through an extensive study of combustion phenomena in the straight-through type radiant heater. Using this parameter, the mass flow rates of each constituent are expressed as (Chapman *et al.*, 1988):

$$\dot{m}_{fuel} = \dot{m}_{fuel\_initial}(1-k) \tag{2.6}$$

$$\dot{m}_{air} = \dot{m}_{air\_initial}(1-\Phi k) \tag{2.7}$$

$$\dot{m}_{product} = \dot{m}_{fuel\_initial} + \dot{m}_{air\_initial} - (\dot{m}_{fuel} + \dot{m}_{air}) \tag{2.8}$$

where Φ is the equivalence ratio.

With the assumption of an absorbing-emitting medium, the radiative mode of energy transfer appearing in equation (2.3) can be written as (Chapman *et al.*, 1988):

$$q_{rad_i} = \frac{\varepsilon_{w_i}\sigma(\varepsilon_g T_g^4 - \alpha_g T_w^4)}{1-(1-\varepsilon_{w_i})(1-\alpha_g)} \tag{2.9}$$

Neglecting axial conduction, an energy balance on the tube wall gives the following (Chapman *et al.*, 1988):

$$h_i(T_g - T_w) + q_{rad_i} = \frac{r_o}{r_i}[h_o(T_w - T_{surr}) + q_{rad_o}] \tag{2.10}$$

The convective heat transfer coefficient, h_o, was obtained by assuming free convection at the outer tube surface. A small object in a large isothermal enclosure was assumed to estimate radiative transfer from the tube wall to the surroundings. Chapman *et al.* (1988) solved equations (2.1) through (2.3) with the numerical predictor-corrector method. The gas emissivity and absorptivity in equation (2.9) were obtained with the aid of a temperature and the pressure-path length product that had been studied by Hottel (1954). Chapman *et al.* (1988) obtained the local tube wall temperature by solving equation (2.10) with an under-relaxed Newton-Raphson iteration during each predictor-corrector step.

2.1.3 Heat Transfer from Direct High-Temperature Radiant Heaters

A direct radiant surface combustion heater consists of a plenum chamber, porous surface plate, and reflector around the surface plate. Pre-mixed air and hydrocarbon gas enter the plenum behind the surface plate, and combustion occurs within or at the porous surface plate. The flow rate and ratio of air to fuel of the mixture noticeably affect the burning characteristics of the heater (Chapman *et al.*, 1990). The combustion flame incandesces the porous surface plate and causes the radiant intensity to propagate into the surroundings. Both direct and reflected radiant intensity reach the occupants as the primary heat transfer mode. The higher temperature of the surface plate, however, raises the surrounding temperature through convection.

2.1.4 Mathematical Model of Direct High-Temperature Radiant Heaters

Heat transfer modeling of a direct type heater highly depends on the flame behavior of the burner surface. The porous structure of the burner surface is almost always inhomogeneous, which causes non-uniformity of the burner surface temperatures (Severens *et al.*, 1995). When the fuel-to-air ratio is held constant, the flow velocity of the gas mixture at the burner surface controls the flame behavior of the burner. Basically, three different situations of flame behavior can occur when the gas mixture flow velocity is varied.

Severens *et al.* (1995) studied the operation of a porous surface burner for a wide range of flow velocities at the surface. First, when the flow velocity is relatively low, the location of the combusting flame is within the porous burner surface. With increasing flow velocity, the flame location moves toward the burner surface. Usually, at ideal operation, the flame is stabilized at or just beneath the burner surface because conduction from the flame to the burner surface is optimal and the burner surface temperature is among the highest. This occurs at a flow velocity much lower than the adiabatic flow velocity (Severens *et al.*, 1995). Finally, as the flow velocity approaches the adiabatic flow velocity, the flame departs and is blown off the surface. The burner surface temperature continues to decrease during this transition. Because of non-uniformity of the porous structure, this transition of flame behavior does not occur simultaneously for the entire surface. When the flames over the entire surface leave the surface of the burner plate at a high-flow velocity, conduction from the flame to the burner is nearly zero. The burner surface no longer radiates at this condition.

In the Severen *et al.* study (1995), an important relationship between the pressure drop through the porous burner plate and the flame behavior was observed. The viscosity and density of the gas mixture were a function of temperature. Temperature dependence of the gas mixture's density and viscosity was accounted for by the ideal gas law and an empirical study by Bird *et al.* (1960):

$$\rho(x) = \rho_0 \frac{T_{g,0}}{T_g(x)} \tag{2.11}$$

$$\mu(x) = \mu_0 \left(\frac{T_g(x)}{T_{g,0}} \right)^m \tag{2.12}$$

where the subscript, 0, indicates the mixture state entering the porous plate, and the temperature varies at any position x from the entrance of the pores. The exponent m was found to be between 0.6 and 0.7 (Bird *et al*., 1960). Based on conservation of mass, the mixture velocity through the plate changes as:

$$u(x) = u_0 \frac{\rho_0}{\rho(x)} \tag{2.13}$$

The rate of pressure drop of the gas mixture at any location x can be expressed as (Severens *et al*., 1995):

$$\frac{dp}{dx} = c_1 \mu_0 u_0 \left(\frac{T_g(x)}{T_{g,0}} \right)^{m+1} + c_2 \rho_0 u_0^2 \frac{T_g(x)}{T_{g,0}} \tag{2.14}$$

where coefficients c_1 and c_2 are determined by the geometric configuration of the porous structure. The integration of equation (2.14) requires finding the mixture temperature variance within the porous plate. Assuming combustion occurs outside of the porous plate, the energy balance within the plate yields (Severens *et al*., 1995):

$$\phi \left[\rho_0 \left(\frac{u_0}{\phi} \right) c_p \frac{\partial T_g}{\partial x} - \frac{\partial}{\partial x} \left(k_g \frac{\partial T_g}{\partial x} \right) \right] = hS(T_s - T_g) \tag{2.15}$$

$$-(1-\phi) \frac{\partial}{\partial x} \left(k_s \frac{\partial T_s}{\partial x} \right) = -hS(T_s - T_g) \tag{2.16}$$

where T_s, k_s, k_g, c_p, h, and S are the solid temperature, solid thermal conductivity, gas thermal conductivity, gas specific heat, heat transfer coefficient within the porous structure, and the specific wetted surface per unit volume, respectively. The thermal conductivity of the gas may include the effect of radiation within the plate. The gradient of porosity, ϕ, is neglected in the above equations. Provided that c_p, k_g, k_s, and h are independent of temperature, and radiation takes place only at the surface of the plate, a fourth order differential equation can be obtained (Severens *et al*., 1995):

$$\rho_0 c_p u_0 \frac{\partial T_{g,s}}{\partial x} - \left[\phi k_g + (1-\phi)k_s\right]\frac{\partial^2 T_{g,s}}{\partial x^2}$$

$$-\rho_0 c_p u_0 \frac{\phi(1-\phi)}{hS} k_s \frac{\partial^3 T_{g,s}}{\partial x^3} + k_g k_s \frac{\phi(1-\phi)}{hS}\frac{\partial^4 T_{g,s}}{\partial x^4} = 0 \tag{2.17}$$

where $T_{g,s}$ denotes T_g or T_s. Applying corresponding boundary conditions and neglecting insignificant terms based on experiment observations, the solution to equation (2.16) can be approximated with a block profile that gives (Severens *et al*., 1995):

$$T_g(x) = \begin{cases} T_{g,0} & \text{if} \quad 0 < x < L-\delta \\ T_{g,surf} & \text{if} \quad L-\delta < x < L \end{cases} \tag{2.18}$$

where L is the thickness of the plate, and δ is defined as (Severens *et al*., 1995):

$$\delta = \frac{\phi k_g + k_s(1-\phi)}{\rho_0 u_0 c_p} \tag{2.19}$$

The general solution form for equation (2.17) is a polynomial and consists of four terms in which each term is a product of a constant and an exponential. Upon investigating the boundary conditions to come to the solution of (2.18), it was found to be reasonable to assume $T_{s,surf} \cong T_{g,surf}$ (Severens *et al*., 1995). With the assumption of one-dimensional flame behavior and energy consumption by radiation occurring only at the surface of the burner plate, the energy balance at the burner surface yields (Severens *et al*., 1995):

$$\rho_0 u_0 c_p (T_b - T_b') = \varepsilon\sigma(T_{s,surf}^4 - T_{surr}^4) \tag{2.20}$$

where T_b, T_b', and T_{surr} are the adiabatic, non-adiabatic, and surroundings temperatures, respectively. The variable ε represents the emissivity of the burner surface, and σ is the Stefan-Boltzmann constant. In equation (2.20), a constant specific heat and the emissivity for the temperature range between T_b and T_b' are assumed. A burner-stabilized flame occurs when the gas mixture velocity is at a non-adiabatic velocity of v_L'. Many researchers have studied the relationship between the non-adiabatic flame temperature and velocity. Among them, Kaskan (1967) empirically found the following relationship:

$$u = ke^{-E_a/2RT_b'} \tag{2.21}$$

The value of the coefficient, k, with an effective activation energy, E_a, was obtained through experiments by Kasan (1967). The parameter R that appears in equation (2.21) is the universal gas constant. Equation (2.21) is valid only when the reaction takes place outside the porous plate (Severens *et al.*, 1995). The relation between the adiabatic temperature and velocity can be found (Severens *et al.*, 1995):

$$\frac{v_L'}{v_L} = \exp\left(-\frac{E_a}{2RT_b'} + \frac{E_a}{2RT_b}\right) \tag{2.22}$$

Combining equations (2.20) and (2.22) with experimentally determined values of T_b' and v_L gives the surface temperature as a function of the gas mixture velocity (Severens *et al.*, 1995):

$$T_{s,surf}^4 = \begin{cases} T_{g,0}^4 + \dfrac{\rho_0 u_0 c_p T_b}{\varepsilon\sigma}\left(1 - \dfrac{E_a}{2RT_b \ln\left(\dfrac{u_0}{v_L}\right)}\right) & \text{if } u_0 < v_L \\ T_{g,0}^4 & \text{if } u_0 > v_L \end{cases} \tag{2.23}$$

Using this series of equations allows one to model a direct, high-temperature heater.

2.2 Considerations for Radiant Heater Applications

The most attractive advantage of a high-temperature radiant heater is its capability to supply heat to occupants without having to use the surrounding air as the medium of energy transfer. This is the major reason why high-temperature radiant heaters have been utilized for large open spaces such as aircraft hangars or storage spaces where large volumes of air are present. When these large spaces have a high air change rate per hour, radiant heating is considered more energy efficient than warm air. To optimally implement radiant heating, however, three factors must be considered: 1) the building and energy consumption; 2) the uses and placement of a radiant heater; and 3) ventilation.

2.2.1 Building and Energy Consumption

The *ASHRAE Handbook of Fundamentals* (1993) outlines engineers' widely-accepted strategies for modeling systems and estimating energy usage of various heating system designs. Following the ASHRAE standardized methods, a heating design guidebook published by Solaronics, Inc. (1994a/b), a radiant heater manufacture, summarizes radiant heater system design. Based on the first law of thermodynamics, determination of the amount of heat required to accomplish a desired heating level for any space relies upon an estimation of the space heat loss. Estimation of heat loss involves obtaining the total loss through the walls, roof, and floor of the space to be heated, and the amount of air passing through the space per unit time (Solaronics, 1994a/b). To accomplish this, a complete survey of the space to be heated is necessary. The survey includes desired inside temperature, outside design temperature, building construction, and anything that affects the rate of air change per hour.

To determine the U-value for each wall, roof, and floor the building construction must be inspected. The U-value is the inverse of thermal resistance of the material. Hence, a better insulating material results in a smaller U-value. Lists of U-values for different materials are available in the *ASHRAE Handbook of Fundamentals* (2001). The desired inside temperature depends on usage of the building and the customer's preference. According to Solaronics (1994 a/b), the desired inside temperature when using a radiant heating system can be about 10°F lower than one for a conventional warm-air heating system to achieve the same level of thermal comfort. This decrease is because the comfort level measurement should be based on the operative temperature rather than warm-air temperature in the case of radiant heating. The outside design temperature for different cities can be found in the *ASHRAE Handbook of Fundamentals* (2001). The total transmission loss for the building then can be calculated by the following expression:

$$q_{transloss} = \sum_{i=1}^{N} U_i A_i (T_{inside} - T_{outside}) \tag{2.24}$$

where N is the number of enclosure elements of the room that is normally six, and U_i and A_i are the U-value and area of the corresponding elements, respectively.

The heat loss through the exchange of room air is based on the estimation of air change rate and infiltration rate. The numbers of doors, their frequency of use, and any powered exhaust are the main factors used to determine the air change rate and recommended minimum rate to maintain the room thermally comfortable. The heat lost through air change is a function of: 1) the product of the air change rate and infiltration rate; 2) air specific heat; and 3) design temperature difference between inside and outside. In a general thermodynamics calculation, this is expressed based on mass flow rate. It can be also written on a volumetric flow basis that is used to describe either air change rate or infiltration rate:

$$q_{airloss} = \dot{V}c(T_{inside} - T_{outside}) \tag{2.25}$$

where c is the specific heat of air on a volumetric basis at standard temperature and pressure, and can be obtained using the ideal gas law. The sum of the transmission loss and air loss is the total heat loss for the building. This is not exactly the same, however, as the necessary heat input to maintain the desired inside temperature if there is a significant amount of steady heat gain involved. Heat gains are energy gains from lights, equipment, occupants and solar radiation transmitted through windows. The data to estimate these heat gains are also available in the *ASHRAE Handbook of Fundamentals* (2001). Finally, the required heat input to accomplish the design inside temperature can be expressed as:

$$q_{input} = \frac{1}{\eta}(q_{transloss} + q_{airloss} - q_{heatgain}) \tag{2.26}$$

where η is the efficiency of the radiant heaters. The appropriate heater size, therefore, would be the product of the heat input and the efficiency.

Based on this design of radiant heating system, yearly energy consumption could also be obtained by using the ASHRAE degree-day method. With heat gain, the balance point temperature must be determined to compute the yearly energy consumption. The balance point temperature is defined as (ASHRAE, 2001):

$$T_{bal} = T_{inside} - \frac{q_{heatgain}}{K_{tot}} \tag{2.27}$$

where parameter K_{tot} is the sum of the total heat loss coefficient for the building, which is the sum of the product of U-value, and corresponding area for each enclosing component of the building. Heating is only necessary when $T_{outside}$ is lower than this T_{bal} (ASHRAE, 2001). Using this balance point temperature, the yearly energy consumption can be expressed as (ASHRAE, 2001):

$$Q_{yr} = \frac{K_{tot}}{\eta} \int [T_{bal} - T_{outside}(t)]^{+} dt \tag{2.28}$$

The + sign indicates that only the positive temperature difference should be taken. Equation (2.28) is the time integral of the energy consumption rate over a year. Here, the outside temperature is a function of time varying seasonally. To approximate the integral, the average outside temperature, daily or hourly, must be summed over the entire heating season (ASHRAE, 2001). These are termed degree days or degree hours, respectively. The degree days for heating can be expressed as (ASHRAE, 2001):

$$DD_h(T_{bal}) = (1day)\sum_{days}(T_{bal} - T_{outside})^{+} \tag{2.29}$$

This quantity of degree days for different cities is also available in the *ASHRAE Handbook of Fundamentals* (2001). Then, the integral of equation (2.28) can be replaced by:

$$Q_{yr} = \frac{K_{tot}}{\eta} DD_h(T_{bal}) \tag{2.30}$$

This method of evaluating yearly energy consumption is appropriate when the system efficiency and usage of the building is steady.

2.2.2 Uses and Placement of Radiant Heaters

Radiant heaters are popular for heating a specific area or spot as opposed to an entire space. Spot and area heating actually refer to different areas for which the radiant intensity field is desired. Spot heating is directed toward a specific area where occupants are most often present. The goal of spot heating is to maintain no net heat loss of an individual surface by providing heat that is equal to the surface heat loss (Solaronics, 1994a/b). Area heating refers

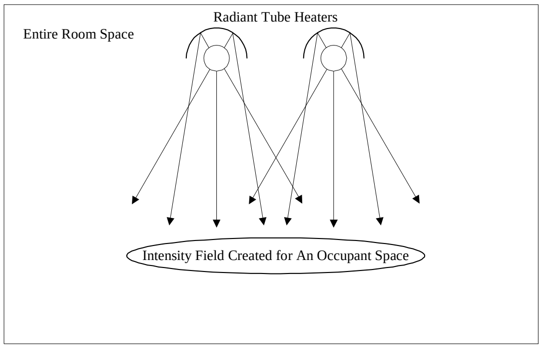

Figure 6: Creation of Intensity Field.

to a section or zone of an occupied building and typically represents more square feet of space than that of spot heating.

Figure 6 illustrates this concept and explains why radiant heaters are so popular for spot heating. The intensity that comes from the emitting surface of the radiant heater is specific in direction and is dispersed as it travels further from the surface.

Regardless whether a high-temperature radiant heater is used for an area or spot, the body heat loss must be taken into account. Body heat loss depends upon: 1) the temperature; 2) the flow conditions of the surrounding air; and 3) the clothing and activity of the individual(s). A first law energy balance can be used to estimate the body surface heat loss and determine heater size in order to provide a desirable amount of heat to the occupant. The optimal location of the heater depends on the geometry of the reflector.

2.2.3 Ventilation

The porous structure of the burning surface induces a continuous conduction from the flame to the surface plate. Relatively low flow velocity appreciably lowers the flame temperature compared to other conventional combustion processes and results in a large reduction of polluting products such as nitrogen oxide (Severens *et al.*, 1995). Regardless of the significant decrease in polluting emissions, use of direct high-temperature radiant heaters still requires a higher rate of ventilation than indirect high-temperature radiant heaters. This is because the combusting gases of a direct radiant heater are directly exposed to the room air, whereas the combustion gases from an indirect radiant heater are exhausted to the atmosphere.

Since increased ventilation is required for a room with a direct radiant heater, the result is that a lower room temperature. A lower room temperature, in turn, influences the estimation of heat loss of the occupants or heat loss of the building. This difference must be taken into account when designing calculations for a direct radiant heating system, but is not a design consideration for indirect radiant heating systems.

An obvious disadvantage of a direct radiant heater is the greater energy consumption because of the higher rate of air change per hour. An advantage of direct radiant heaters over indirect radiant heaters is that direct radiant heaters have a lower initial cost because no exhaust piping is needed. Since the combustion in a direct radiant heater occurs directly with the room air, the room air is more humid, which may contribute to a better comfort level.

The various applications of high temperature radiant heaters drives the process that will be used to model those heaters. For example, the model needs to incorporate the impact of ventilation, as well as the heat transfer rates from the surfaces of the heater surfaces.

3.0 Heat Transfer and Mathematical Models

This section describes the variety of mathematical models that can be used to simulate the impact of high temperature radiant heaters on thermal comfort.

3.1 Radiative Transfer

The radiative transfer equation is the most general technique for modeling and predicting radiative heat transfer in an enclosed space. To solve this equation, knowledge of view factors is not required. In fact, view factors can be calculated by solving for the radiative heat transfer. A drawback, however, is that a computer simulation is virtually required due to the difficultly of the equation. Several such computer solution techniques have been developed over the last several decades.

3.1.1 Radiative Transfer Equation

The radiative transfer equation (RTE) solves directly for the radiant intensity at each point, wavelength, and direction in the enclosed space. Once the intensity field is known, the local radiant heat fluxes can be calculated by integrating the intensity over the solid angle. This process sounds complex, and indeed it is. For the time being, consider the set of equations needed to complete this process with the understanding that a computer solution for the radiative transfer equation will follow.

The general form of the radiative transfer equation (Viskanta and Mengüc, 1987; Siegel and Howell, 1981; Özisik, 1977) is given by:

$$(\nabla \bullet \vec{\Omega}) I_\lambda(\vec{r},\vec{\Omega}) = \mu \frac{\partial I_\lambda}{\partial x} + \xi \frac{\partial I_\lambda}{\partial y} + \eta \frac{\partial I_\lambda}{\partial z} = -(\kappa_\lambda + \sigma_{s,\lambda}) I_\lambda + \kappa_\lambda I_{b,\lambda} + \frac{\sigma_{s,\lambda}}{4\pi} \int_{\Omega'} \Phi(\Omega' \rightarrow \Omega) I_\lambda(\Omega') d\Omega' \tag{2.31}$$

The intensities and properties in equation (2.31) have the subscript λ to designate that each quantity is a function of wavelength. The first term in the equation represents the spatial distribution of the radiant intensity. The variables μ, ξ, and η are the directional cosines that describe the direction of the radiant intensity. The variables κ and σ represent the medium absorption coefficient and the medium scattering coefficient.

The absorption coefficient must be greater than zero. As the absorption coefficient increases, the more the medium behave toward radiation and participate in the radiation exchange process. The participating medium can either increase or decrease the intensity magnitude, which depends upon the absorption coefficient, the medium temperature, and the temperature of the surrounding.

The scattering coefficient is probably one of the least understood parameters in the radiant heat transfer field. The scattering coefficient describes how the intensity in a specific direction is scattered into different directions. The intensity from a different direction also can be scattered into the direction of concern. While the scattering coefficient is important in industrial processes such as glass making, it has little relevance in the building environment and can be assumed to be zero. For the special case of a typical occupied room where the absorption and scattering coefficients can be assumed zero, the equation reduces to:

$$\mu \frac{\partial I}{\partial x} + \xi \frac{\partial I}{\partial y} + \eta \frac{\partial I}{\partial z} = 0 \tag{2.32}$$

As will be shown later, the water vapor content of the air can play a significant role in radiative transfer throughout the room. Consequently, equation (2.32) is not recommended as a general form of the radiative transfer equation, but rather equation (2.31) without the scattering term is the preferred form. Several solution methods exist to solve this non-linear equation.

3.1.2 Solution Techniques for the Radiative Transfer Equation

In most cases, the RTE that precisely represents a practical engineering system does not have a closed-form analytical solution because of the multidimensional and spectral nature of radiation in engineering systems and its property dependence on position, local temperature, and local composition (Viskanta and Ramadhyani, 1988). In addition, the physical and radiative property data are not adequate to develop an exact solution (Viskanta and Ramadhyani, 1988). Furthermore, an inhomogeneous gas mixture case requires an enormous amount of computations for an RTE solution. These constraints have prevented engineers from developing a general solution method for the RTE.

A number of techniques that evaluate the solution, however, have been developed. All of these employ simplifying assumptions in order to reach an RTE solution with an acceptable level of errors. Each method consists of a different modeling scheme and utilizes different assumptions. The best method to select depends on: 1) the physical nature of the system; 2) the medium radiation characteristics; 3) the desired accuracy level; and 4) computer resource availability. Each method has its advantages and disadvantages which should be taken into consideration (Viskanta and Ramadhyani, 1988).

Five methods to solve the RTE are the: 1) mean beam length method; 2) Hottel's zone method; 3) spherical harmonics method and moment method; 4) Monte Carlo method; and 5) discrete ordinates method. A short discussion of each method follows, but does not focus on the detailed derivations of each.

Mean Beam Length Method

Hottel and Sarofim (1967) first evolved the notion of mean beam length to determine radiative transfer from the products of combustion to its enclosure (Modest, 1993). The temperature of the gas was assumed uniform, and the surfaces of the enclosure were taken to be black at first. The method also could be applied to a gray surface enclosure with slightly more difficulty (Modest, 1993), but this discussion only introduces the fundamentals with a black wall enclosure. This method, while considered classic, has become more obsolete with the advancement of computers. Nevertheless, the concept of mean beam length is important since it sometimes appears in other methods of radiative heat transfer (Modest 1993).

Assume a non-scattering gas at a uniform temperature in a black surface enclosure shown in Figure 7. Referring to Figure 7, the spectral heat flux from an infinitesimal gas volume dV to a local area dA can be expressed as (Modest, 1993):

$$q_\lambda(r_s) = I_{b,\lambda} \int_V e^{-\kappa_\lambda s} \frac{\kappa_\lambda \cos\theta \, dV}{S^2} \qquad (2.33)$$

where κ_λ is a spectral absorption coefficient of the gas. This volumetric integral is not easy to evaluate for most geometries. If the entire volume has a hemispheric shape and radiates toward the center of the base as shown in Figure 8, then S is equal to r and dV can be written as $r^2 \sin\theta \, dr d\theta d\phi$.

In addition, including the fact $d\Omega = \sin\theta \, d\theta d\phi$, equation (2.22) becomes:

$$q_\lambda = I_{b,\lambda} \int_{\Omega=0}^{2\pi} \int_{r=0}^{R} e^{-\kappa_\lambda r} \kappa_\lambda \cos\theta \, dr d\Omega \qquad (2.34)$$

Evaluating this integral yields (Modest, 1993):

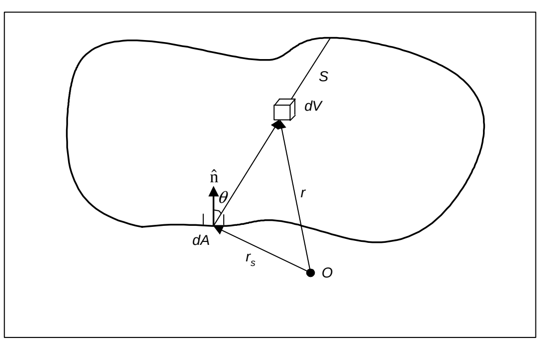

Figure 7: Isothermal Gas in a Black Enclosure (Modest 1993).

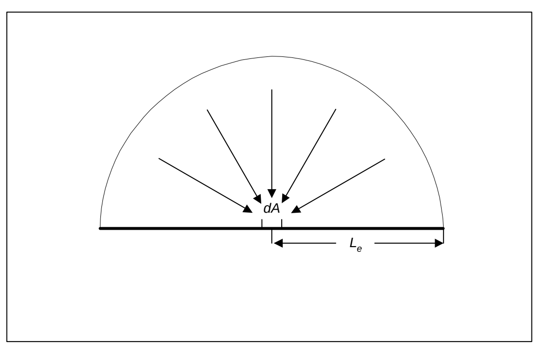

Figure 8: Radiation of Equivalent Hemisphere Surface toward the Base Center (Modest 1993).

$$q_\lambda = \pi I_{b,\lambda}(1 - e^{-\kappa_\lambda R}) = \pi I_{b,\lambda}\varepsilon_\lambda \tag{2.35}$$

For R in equation (2.35), there is a value that makes numerical evaluation of equation (2.34) and equation (2.35) exactly equivalent. In other words, the radiative heat flux arriving from a volume of arbitrary shape and the radiative heat flux from a hemispherical volume with radius R have the same magnitude. This specific value of the radius is called the mean beam length, and is denoted by L_e. Hence, the mean beam length, L_e, is a quantity that satisfies the following relation (Modest, 1993):

$$\frac{q_\lambda}{\pi I_{b,\lambda}} = 1 - e^{-\kappa_\lambda L_e} = \frac{1}{\pi}\int_V e^{-\kappa_\lambda S}\frac{\kappa_\lambda \cos\theta\, dV}{S^2} \tag{2.36}$$

The evaluation of the above equation is rather difficult; but becomes much easier for a specific case. Suppose the medium is optically thin; or in other words, the product of the absorption coefficient and the medium characteristic length is less than or equal to one. In addition, if the any higher than first order terms of the absorption coefficient are neglected during the process of expanding the exponent, then the following simple relation holds (Modest, 1993):

$$L_0 = 4\frac{V}{A_s} \tag{2.37}$$

where L_0 is the limited value for optically thin media that is equivalent to the partial pressure of the radiatively participating medium approaching zero (Viskanta and Ramadhyani, 1988); and V and A_s are the volume of the medium and its surface area, respectively. Hottel and Sarofim (1967) found that since the radiative heat flux has insignificant dependence on the spectral variances of the mean beam length L_e, it could be replaced by the constant value of the average mean beam length, L_m (Modest, 1993). The relation between L_e and L_m are:

$$L_m \approx 0.9L_e = 3.6\frac{V}{A_s} \tag{2.38}$$

Using this idea of the mean beam length, the net radiative exchange between the gas and the surrounding black walls can be written as (Viskanta and Ramadhyani, 1988):

$$Q_{g\leftrightarrow s} = \left[\varepsilon_g(L_m)E_b(T_g) - \alpha_{gs}(L_m)E_b(T_s)\right] \qquad (2.39)$$

where α_{gs} is the gas absorptivity for irradiation from a wall surface having its temperature of T_s.

Hottel's Zone Method

For radiation heat transfer calculations, Hottel's zone method has been one of the most accepted techniques since its introduction in 1967 by Hottel and Sarofim (Viskanta and Ramadhyani, 1988). The method presumes the system volume and surfaces are composed of a number of zones with uniform temperatures and radiative properties for each zone. A zone could be a surface or a volume. The method employs a concept of direct exchange areas for surface-surface, volume-surface, and volume-volume exchange. Although the method is applicable to a system having a non-radiating participating medium, this discussion presents a general formulation for a gray absorbing and emitting medium in a gray enclosure.

Assume a system is divided into M volume zones and N surface zones. Then, direct exchanges for surface-to-surface, volume-to-surface, and volume-to-volume are defined respectively as (Hottel and Sarofim, 1967):

$$\overline{s_i s_j} = \int_{A_i}\int_{A_j} \frac{\tau(S)\cos\theta_i \cos\theta_j}{\pi S^2} dA_j dA_i \qquad (2.40)$$

$$\overline{g_i s_j} = \int_{V_i}\int_{A_j} \frac{\kappa_i \tau(S)\cos\theta_j}{\pi S^2} dA_j dV_i \qquad (2.41)$$

$$\overline{g_i g_j} = \int_{V_i}\int_{V_j} \frac{\kappa_i \kappa_j \tau(S)}{\pi S^2} dV_j dV_i \qquad (2.42)$$

where $\tau(S)$, which appears in each equation, is the transmssivity of the medium. This can be written as:

$$\tau(S) = e^{-\int_0^S \kappa dS} \qquad (2.43)$$

where κ is the absorption coefficient that varies depending on each zone. The assumption of a gray medium holds for the law of reciprocity (Hottel and Sarofim, 1967), which states that:

$$\overline{s_is_j} = \overline{s_js_i},\ \overline{g_is_j} = \overline{s_jg_i},\ \overline{g_ig_j} = \overline{g_jg_i} \tag{2.44}$$

For an isothermal enclosure, all the areas contributing to the flux from any one zone to each of the other zones are equal to the energy originating from that zone. The following relations for the surface zones and the volume zones respectively are (Hottel and Sarofim, 1967):

$$\sum_{j=1}^{N}\overline{s_js_i} + \sum_{k=1}^{M}\overline{g_ks_i} = A_i, \quad i = 1,2,\ldots,N \tag{2.45}$$

$$\sum_{j=1}^{N}\overline{s_jg_i} + \sum_{k=1}^{M}\overline{g_kg_i} = 4\kappa_iV_i, \quad i = 1,2,\ldots,M \tag{2.46}$$

The equation of the radiosity, W, which is the sum of emission and reflection, for surface i of N surface zone that surround a volume zone may be expressed as (Hottel and Sarofim, 1967):

$$\sum_{j=1}^{N}\left[\overline{s_is_j} - \delta_{ij}\frac{A_j}{\rho_j}\right]W_j = -\frac{A_i\varepsilon_iE_{b,i}(T_i)}{\rho_i} - \overline{g_js_i}E_{b,g}(T_g) \tag{2.47}$$

where δ, called the Kronecker delta, has the value of zero except when $i = j$, which then takes a value of one. For surface j with $E_{b,i}$ equal to one and zero for all other black body emissive fluxes, solving equation (2.47) yields the total exchange area between i and j surfaces (Hottel and Sarofim, 1967):

$$\overline{S_iS_j} = \frac{A_j\varepsilon_j}{\rho_j}\left({}_iW_j - \delta_{ij}\varepsilon_i\right) \tag{2.48}$$

With the same manner, the total exchange areas for volume-to-surface and volume-to-volume could be obtained respectively as follows (Hottel and Sarofim, 1967):

$$\overline{G_iS_j} = \frac{A_j\varepsilon}{\rho_j}\left({}_{g,i}W_j\right) \tag{2.49}$$

$$\overline{G_i G_j} = \overline{g_i g_j} + \sum_{i=1}^{M} \overline{s_k g_j}({}_{g,i} W_k) \tag{2.50}$$

where g,i is the volume zone i.

Obtaining these total exchange areas allows the expression of the net radiative exchange for each zonal element with the other elements within the enclosure. For instance, the net radiative exchange between surface i and the total of N surfaces in the enclosure would be expressed as (Viskanta and Ramadhyani, 1988):

$$Q_i = \sum_{j=1}^{N} \left(\overline{S_i S_j}\right)\left[E_{b,s}(T_{s,i}) - E_{b,s}(T_{s,j})\right] \tag{2.51}$$

The net radiative exchanges between volume-to-surface and volume-to-volume also could be found in a similar manner (Viskanta and Ramadhyani, 1988).

One advantage of the zone method is the possibility of highly accurate solutions (Viskanta and Ramadhyani, 1988). By taking into account non-uniformities of temperature and composition in the system, the method can theoretically predict exact solutions with a large number of zones. Disadvantages of the method are the excessive computational time required to obtain such accuracy, and the lack of applicability for a system with complex geometry. When system geometry is complicated, then computations for some factors such as direct exchange areas become extremely difficult. Even though these disadvantages are still present, many engineers have modified the original version of the zone method to be more suitable for different type of radiative transfer problems.

Spherical Harmonics Method (P_N Approximation) and Moment Method (Differential Approximation)

The RTE for a practical engineering system generally does not have a closed-form analytical solution to obtain the radiative intensity because it tends to have a form of integro-differential equation having several independent variables (Modest, 1993). The spherical harmonics method, which is a differential approximation, permits an approximate solution with arbitrary accuracy. To provide such an approximation, the method employs a series expansion to express the radiative intensity that results in transformation of the RTE into a set of simultaneous partial differential equations. The spherical harmonics method uses spherical harmonic orthogonality, whereas the moment method does not (Modest, 1993). The two methods are equivalent with a P_1 approximation and the lowest order of the moment method (Özişik, 1973), but the spherical harmonics method goes further and allows for higher order approximations. In radiative transfer problems P_1 and P_3 approximations most commonly are used. Neutron transport theory suggests that any order of even number approximations tend to have lower accuracy; and therefore, should not be used for practical applications (Modest, 1993).

For a P_1 approximation, a single elliptical partial differential equation describes the zero[th]-order moment of the spectral intensity, G_λ, (Viskanta and Ramadhyani, 1988):

$$\nabla^2 G_\lambda = A_\lambda \left[G_\lambda - 4\pi I_{b,\lambda}(T) \right] \tag{2.52}$$

The definitions of A_λ and G_λ appearing in equation (2.52) are:

$$G_\lambda = \int_{\Omega=4\pi} I_\lambda d\Omega, \qquad A_\lambda = 3\beta_\lambda^2 \left(1-\omega_\lambda\right)\left[1-\omega_\lambda\left(f_\lambda + g_\lambda - f_\lambda g_\lambda\right)\right] \tag{2.53}$$

where β_λ is the extinction coefficient, ω_λ is the scattering albedo, and f_λ and g_λ are phase function parameters. The delta-Eddington phase function was utilized for the above approximation (Mengüc and Viskanta, 1985). With the aid of the approximation, the evaluation for the local radiative flux yields (Viskanta and Ramadhyani, 1988):

$$\vec{F} = -\frac{1}{3}\int_0^\infty \left(\frac{1}{\beta_\lambda}\right) \nabla G_\lambda \, d\lambda \tag{2.54}$$

When higher order moments of intensity are used, such as a P_3 approximation, the number of elliptical partial differential equations increases, and this results in more complex equations that must be solved. Low-order approximations are accurate only for optically thick media (Modest, 1993). For instance, the P_1 approximation yields an accurate solution when the optical dimension (product of the extinction coefficient and characteristics length) of the medium exceeds two (Viskanta and Ramadhyani, 1988). In the case of a P_3 approximation, the solution is accurate when the medium optical dimension is greater than or equal to 0.5 (Mengüc and Viskanta, 1985). In spite of increased complexity for higher order approximations, improvement of accuracy in resulting solution is rather slow (Modest, 1993).

Monte Carlo Method

The Monte Carlo method is a numerical method that depends on statistical probabilities. This method could be employed not only to solve radiative transfer problems, but also to solve many different mathematical problems. In radiative transfer problems, the method is often used with the zonal method (Chapman and DeGreef, 1997). Since the Monte Carlo method has more than one way to formulate mathematical or engineering solutions (Viskanta and Ramadhyani, 1988), no specific modeling scheme is presented.

The attempt of Howell and Perlmutter to solve a radiative transfer with a non-participating medium in enclosures was one of the earliest applications of this method to thermal radiation problems (Modest, 1993). The Monte Carlo method utilizes statistical probabilities to model radiative phenomena of emission, reflection, and absorption. The passages of bundles of a photon that result from surface emissions are each traced until it interacts with another surface as absorption or reflection. These surfaces could be the surfaces of the volume element as introduced in Hottel's zone method. A random number generator is employed to predict the direction of the photon and whether it would be absorbed or reflected (Brewster, 1992). If the photon is absorbed, then the history of the trace is finalized. If the photon is reflected, then the reflecting angle is obtained through the same process of random number generation. The process is repeated until the photon is absorbed at some surface to end its tracing history (Viskanta and Ramadhyani, 1988).

The Monte Carlo method has considerable advantages. The methodology yields very accurate solutions with increasing surface elements and is applicable to complicated geometries and radiatively participating media. Despite an increase in accuracy desired and in geometric or other complexity, the method requires no significant increase in difficulty of modeling formulation and in computational time. Drawbacks include the heavy reliance upon computer resources, the complicated modeling process even for a simple system, and inherent statistical errors (Howell, 1968; Modest, 1993).

Discrete Ordinates Method

The discrete ordinates method was first applied to neutron transport theory and is described by Carlson and Lathrop (1963). The discrete ordinates method, which is used by the BCAP methodology (Jones and Chapman, 1994; Chapman and Zhang, 1995, 1996; Chapman et al., 1997), considers discrete directions and nodes on the surface, and calculates the radiant intensity at each point and direction. The enclosure space is divided into control volumes. Equation (2.32) is integrated over each three-dimensional control volume. The resulting equation for a gray surface in a discrete direction, *j*, is:

$$\int_z^{z+\Delta z}\int_y^{y+\Delta y}\int_x^{x+\Delta x}\left(\mu\frac{\partial I^j}{\partial x}+\xi\frac{\partial I^j}{\partial y}+\eta\frac{\partial I^j}{\partial z}\right)dxdydz=0 \qquad (2.55)$$

The discrete ordinates method designates the directions for *j*. Higher orders of approximation have more prescribed directions and can increase the accuracy of the results, however, the larger order approximations require more computational time.

The control volume intensity along one side is assumed to be independent of the other two directions. For example, the intensity along the x interface is not affected by the y and z direction (Patankar, 1980). The equation then becomes:

$$\mu^j\Delta z\Delta y(I^j_{x+\Delta x}-I^j_x)+\xi^j\Delta z\Delta x(I^j_{y+\Delta y}-I^j_y)+\eta^j\Delta x\Delta y(I^j_{z+\Delta z}-I^j_z)=0 \qquad (2.56)$$

This equation contains six interface intensities. By assuming that the intensity profile across the control volume is linear, the intensity at the center of the control volume, point *p*, is (Truelove, 1988; Fiveland, 1988):

$$I^j_p=\alpha I^j_{x+\Delta x}+(1-\alpha)I^j_x=\alpha I^j_{y+\Delta y}+(1-\alpha)I^j_y=\alpha I^j_{z+\Delta z}+(1-\alpha)I^j_z \qquad (2.57)$$

The interpolation factor, α, is set equal to 1 to avoid negative intensities, which are physically impossible and yield unstable solutions. Fiveland (1984, 1988) reports that α=1 will always provide positive intensities. Substituting equation (2.56) into equation (2.57) yields:

$$I_p^j = \frac{\mu^j \Delta z \Delta y I_x^j + \xi^j \Delta z \Delta x I_y^j + \eta^j \Delta x \Delta y I_z^j}{\mu^j \Delta z \Delta y + \xi^j \Delta z \Delta x + \eta^j \Delta x \Delta y} \tag{2.58}$$

Equation (2.58) is written for all the discrete directions for each control volume. An S_4 approximation has 24 discrete directions at each control volume. The values for μ^j, ξ^j, and η^j must satisfy the integral of the solid angle over all the directions, the half-range flux, and the diffusion theory (Truelove, 1987, 1988). Table 2.1 gives the values for μ^j, ξ^j, and η^j for the first quadrant. A complete table of values that satisfy these conditions is tabulated and available from Fiveland (1988) and Chapman (1992).

The Δx, Δy, and Δz values are determined by the size of the control volume. The I_x^j, I_y^j, and I_z^j values are known from the previous iteration. Initially, the intensities are set to beginning values. The solution is iterative around a loop from p=1 to p equals the total number of control volumes until the solution converges.

With the known intensity, the incident radiation on the surface can be written as (Siegel and Howell, 1981):

$$q_{rad} = \int_{\Omega'} |\mathbf{n} \bullet \Omega'| I(\Omega') d\Omega' \tag{2.59}$$

For a radiant heat flux in the x-direction, equation (2.59) is approximated using a quadrature (Fiveland, 1988) and becomes:

$$q_{rad} = \sum_j \mu^j I^j w^j \tag{2.60}$$

Table 2.1 First Quadrant Values for Directional Cosines and Weighting Factor.

Ordinate Direction	μ^j	ξ^j	η^j	w^j
1	-0.2959	-0.9082	0.2959	0.5239
2	0.2959	-0.9082	0.2959	0.5236
3	-0.9082	-0.9082	0.2959	0.5236
4	-0.2959	-0.2959	0.9082	0.5236

The values for w^j are given in Table 2.1 and can be used to solve equation (2.60).

The discrete ordinates method has been studied and found to be accurate by Fiveland (1984, 1987, 1988), Fiveland and Jamaluddin (1989), Truelove (1987, 1988), and Sanchez and Smith (1992). The S_4 approximation has been found to be a reasonable compromise between accurate results and a low computational time (Fiveland, 1988). In addition, Fiveland (1984) reported the discrete ordinates method gave more accurate and faster solutions than the P_3 and zonal solutions.

3.2 Relative Humidity and the Absorption Coefficient

Air as a transparent gas is normally considered a radiatively non-participating medium except when its temperature is extremely high. High temperature air has the potential to contain significant amounts of water vapor. This water vapor can absorb and/or emit radiative energy, which affects the radiative heat exchange of a system. For example, the presence of water vapor plays an important role in radiative heat exchange of combustion products. Nevertheless, the effect of absorption by the humid air is more significant than that of emission in the case of radiant heating.

Relative humidity is used to express the amount of water vapor in ambient air. Recall that the absorption coefficient appears in the RTE. This parameter determines the attenuation of the radiative energy by the fluid medium. To incorporate the effect of the air moisture content into the radiative heat exchange analysis, a correlation between the moisture content and the absorption coefficient of the water vapor is desirable.

This section establishes a relationship between relative humidity and the absorption coefficient of the water vapor that can then be used in radiative transfer calculations. First the absorption in gas layers is mathematically examined, and then the absorption coefficient is developed. Partial vapor pressure, relative humidity, and the effect of moist air on absorption are also discussed.

3.2.1 Absorption in Gas Layers

Assume a beam of radiation penetrates a gas layer in a coordinate system, as shown in Figure 9. The spectral intensity along this beam can be written as (Özişik, 1977):

$$\frac{dI_\lambda(S)}{dS} + \kappa_\lambda I_\lambda(S) = 0 \tag{2.61}$$

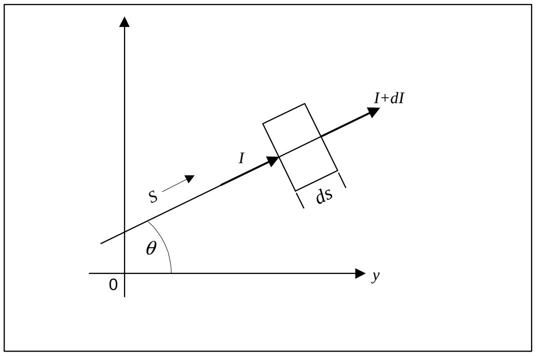

Figure 9: Intensity Beam in a Space (Özişik, 1977).

where κ_λ is the spectral absorption coefficient of the gas layer. The solution to this differential equation with an appropriate boundary condition gives:

$$I_\lambda(S) = I_{\lambda 0} e^{-\kappa_\lambda S} \tag{2.62}$$

where $I_{\lambda 0}$ is the spectral intensity evaluated at $S = 0$. When the thickness of the medium that the beam penetrates is a length L, the spectral intensity at the location L is evaluated as:

$$I_\lambda(L) = I_{\lambda 0} e^{-\kappa_\lambda L} \tag{2.63}$$

Decreasing the intensity from $S = 0$ and $S = L$ results in the spectral radiation attenuated by the gas layer of its thickness L. This can be written as (Özişik, 1977):

$$I_\lambda(0) - I_\lambda(L) = I_{\lambda 0}(1 - e^{-\kappa_\lambda L}) \tag{2.64}$$

Equation (2.64) leads to the spectral absorptivity, α_λ, of the gas layer, which forms the following relation (Özişik, 1977):

$$\alpha_\lambda \equiv 1 - e^{-\kappa_\lambda L} \tag{2.65}$$

Equation (2.65) shows a direct relationship between the absorptivity and the absorption coefficient of the gas layer for a known beam length of radiation. This beam length can be determined by the notion of mean beam length for any desired geometry. In order to solve equation (2.65) for the absorption coefficient, the absorptivity of the gas must be found in some way.

3.2.2 Absorption Coefficient, Absorptivity, and Emissivity of Water Vapor

Despite the direct relationship between the absorption coefficient and the absorptivity for a radiatively participating gas layer has been developed, the evaluation of the gas absorption and emission remains difficult. In fact, quantum physics is involved with the spectral nature of gaseous matter, which contributes to this complexity.

Hottel (1954) solved this difficulty through the development of a simplified method to estimate the total emissivity and absorptivity of water vapor within a non-radiating gas. Total radiative properties are those that are averaged over all wavelengths, and the total quantity is often preferred over spectral properties for typical engineering calculations. In this methodology, the gas was assumed to have a hemispherical volume at a uniform temperature. The emissivity of the vapor was correlated with: 1) temperature; 2) partial pressure; 3) total pressure of the entire gas volume; and 4) the radius of the hemisphere. The experimental results of water vapor emissivity, conducted by Hottel *et al.* (1967), were provided as a chart.

Since these empirical results were based on the total gas pressure of 1 atmosphere, the emissivity obtained from the chart would have to be multiplied by a correction factor for a gas mass with a total pressure other than 1 atmosphere. Hottel *et al.* (1967) also developed a chart of correction factors. Since Hottel's charted values were valid only for a hemispherical gas volume, then the mean beam length must be incorporated for an arbitrary shape of gas mass.

The emissivity for water vapor, obtained from Hottel's (1954xx) charts, are the total spectral value for a given pressure and temperature. They were experimentally measured values that included some extrapolations. Leckner (1972) investigated the water vapor emission and found that the extrapolated values for homogeneous gases from Hottel's charts did not agree well with the calculated values based on statistically available spectral data. He formed a new chart for water vapor emissivity with the same parameters as the ones used in Hottel's chart. Leckner's results agreed well with the ones derived by some other investigators, such as Ludwig *et al.* (19xx) who also studied water vapor emissivity after Hottel (Modest, 1993).

For the purpose of computer programming, Leckner (19xx) also developed a functional expression of the emissivity that was consistent with his results. This expression has less than ±5% maximum error with the chart for temperatures greater than 100°C. His research focues more on higher temperatures of gases and the radiative transfer of combustion products. Some data for the range of room temperatures could be used from these studies.

The functional relationship for the emissivity and absorptivity of water vapor from the revised charts are (Modest, 1993):

$$\varepsilon = \varepsilon(p_g L_m, p, T_g) \tag{2.66}$$

$$\alpha = \alpha(p_g L_m, p, T_g, T_s) \approx \left(\frac{T_g}{T_s}\right)^{0.5} \varepsilon\left(p_g L_m \frac{T_s}{T_g}, p, T_s\right) \tag{2.67}$$

where T_g and T_s are the temperatures of the water vapor and an external black body heat source surface, respectively (Modest, 1993).

3.2.3 Partial Vapor Pressure and Relative Humidity

When using the empirical data, the partial pressure of water vapor must be known to obtain the emissivity and absorptivity for a given state of the gas mixture containing dry air and water vapor. To determine the partial pressure of the vapor within a given moist air, the relative humidity can be a useed. Within a given moist air, the relative humidity measures the ratio of the mole fraction of water vapor to the mole fraction of the maximum moisture possible, which is the saturated condition. The relative humidity, normally denoted by ϕ, is defined as (Moran and Shapiro, 1992):

$$\phi = \left.\frac{y_v}{y_{v,sat}}\right)_{T,p} \tag{2.68}$$

In equation (2.68), y_v is the mole fraction of water vapor in a given moist air, and $y_{v,sat}$ is the mole fraction of the saturated vapor at the same mixture temperature, T, and pressure, p. Because the partial pressure of the water vapor is directly proportional to its mole fraction, equation (2.68) can be written as (Moran and Shapiro, 1992):

$$\phi = \left.\frac{p_v}{p_g}\right)_{T,p} \tag{2.69}$$

where p_v is the partial pressure of the water vapor actually present in the sample air, and p_g is the pressure of the saturated vapor at the temperature and pressure of the sample. Solving equation (2.69) for the partial vapor pressure readily results in:

$$p_v = \phi\, p_g(T, p) \tag{2.70}$$

The saturated vapor pressure can be determined for a given pressure and temperature of the moist air. As such, for the same moist air, the partial pressure of water vapor can be determined for a given relative humidity.

3.2.4 Effect of Moist Air Absorption and Simulation

Using the developed approach to determine the absorption coefficient for the moist air present for a radiant-heating thermal comfort calculation, the RTE that includes the effect of medium absorption can be solved. In radiant heating calculations, the significance of the effect of medium absorption by moist air is of great interest. Unless the effect of radiative energy absorption by the moist air is small enough to be neglected, the absorption coefficient for moist air should be included in calculations when sizing a radiant heater for a desired thermal comfort delivery.

To examine the effect of radiative energy absorption by the moist air, simple radiant-heating models were simulated using a discrete-ordinate module solver. Three sizes of rectangular parallel-piped geometry were used to implement these simulations. The schematic that describes the geometry for the simulations is shown in Figure 10.

The top and bottom surfaces have equal dimensions of 100 m^2, and are maintained the same throughout all simulations. All the surfaces were assumed to be black body. The temperature of the top surface and the other surfaces were kept at 500 K and 290 K, respectively. The total medium pressure was 1 atmosphere. The distance, L, varied with values of 1 m, 5 m, and 10 m. For each distance of L, the amount of radiation from the top surface that reached the center of the bottom surface was simulated for three medium temperatures of 280 K, 290 K, and 300 K. Each of the nine cases was run over a range of relative humidity levels.

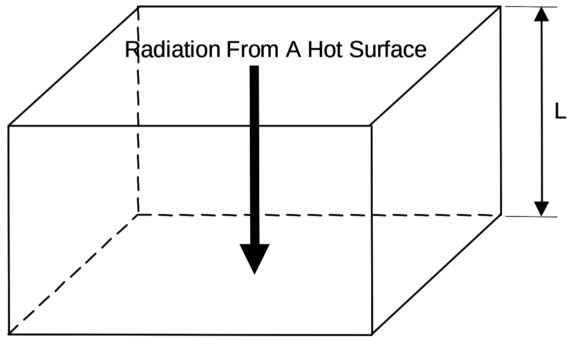

Figure 10: Schematic of Simulation Geometry.

During these simulations, the spectrally averaged absorption coefficient was repetitively evaluated for each scenario. The saturated vapor pressure for each given temperature was directly utilized from a table of saturated vapors under a constant total pressure of 1 atmosphere. The product of this saturated vapor pressure and the relative humidity level gave the partial pressure of the vapor that was present in the medium air. Under the optically thin medium assumption that is almost always valid for a gaseous medium, equation (2.38) was used to evaluate the average mean beam length for a given geometry. Leckner's functional expression of the vapor emissivity in equation (2.67) was used to evaluate the absorptivity. This expression is a set of two second-order polynomials. Leckner's original polynomial expressions to obtain the vapor emissivity of equation (2.66) are:

$$\ln \varepsilon = a_0 + \sum_{i=1}^{2} a_i \lambda^i \tag{2.71}$$

$$a_i = c_{0i} + \sum_{j=1}^{2} c_{ji} \tau^j \tag{2.72}$$

where λ in equation (2.71) and τ in equation (2.72) are defined as:

$$\lambda = \log p_g L_m \tag{2.73}$$

$$\tau = T_g / 1000 \tag{2.74}$$

Nonetheless, $p_g L_m$ in equation (2.73) and T_g in equation (2.74) were replaced by $p_g L_m (T_s / T_g)$ and T_s, respectively, to obtain the vapor absorptivity. The values of coefficients c_{ji} for equation (2.71) are listed in Table 2.2.

Once the absorptivity was determined, equation (2.65) without spectral dependence was solved for the spectrally averaged absorption coefficient with the parameter L being the averaged mean beam length.

Figure 11 contains the nine different plots of the simulations. The quantity on the vertical axis, ψ, is the non-dimensional heat flux, which is defined as the ratio of irradiation flux at the center of the bottom surface to the net radiation flux from the top surface that would occur for the temperature difference between the two surfaces. It is mathematically defined as:

$$\psi = \frac{q_{irradiation}}{\sigma(T_{top}^4 - T_{bottom}^4)} \tag{2.75}$$

Solid lines, coarsely dashed lines, and finely dashed lines represent the cases where the air temperatures are 280 K, 290 K, and 300 K, respectively. Two phenomena can be observed from these plots.

First, as the distance L increased, then resulted in thicker moist air at each relative humidity level. This occurs because less radiation reaches the center of the bottom surface. The increase of saturated vapor pressure means that the higher air temperatures can absorb more water vapor.

For example, when L equals 10 m, only about 93% of radiation flux from the top surface reaches the bottom surface center at zero relative humidity. Compare this to when L equals 1 m with zero relative humidity where almost all the emitted radiation from the top surface is

Table 2.2: Coefficient Values for Equation (2.71) (Leckner, 1972).

i	c_{0i}	c_{1i}	c_{2i}
0	-2.2118	-1.1987	0.035596
1	0.85667	0.93048	-0.14391
2	-0.10838	-0.17156	0.045915

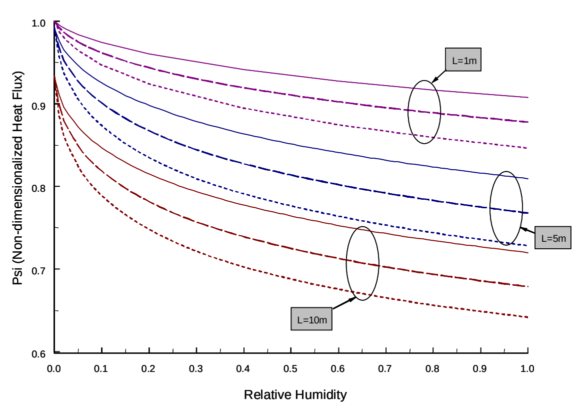

Figure 11: Non-dimensional Heat Flux vs. Relative Humidity.

absorbed by the bottom center surface. As L increases, the radiant beams begin to spread and some hit other walls.

The second observation from Figure 11 is that as the relative humidity increases, less radiation flux arrives at the bottom center for all the cases of air temperature and distance L. This occurs because of an increase in absorption. For example consider the case with a medium temperature of 290 K, a distance of 1 m, and a relative humidity of 70%, which represents a practical case during the winter, only about 90% of the radiation flux reaches the bottom center. In other words, the air absorbs 10% of the radiation flux emitted from the top surface.

A parameter called optical thickness is used to further consider the relationship between absorption and the distance L. Optical thickness is the product of the absorption coefficient and medium characteristic length, where the medium characteristic length is the ratio of the volume, V, and the surface area, A_s, of the medium that is define as:

$$L_c = \frac{V}{A_s} \tag{2.76}$$

The optical thickness is a dimensionless quantity, and physically represents the absorbing density of the medium.

Figure 12 is a plot of change in non-dimensional heat flux with respect to change in optical thickness for the medium temperature of 300K and the distance L of 10m. As expected, when optical thickness increases for any given temperature and distance, then less radiation hits bottom center.

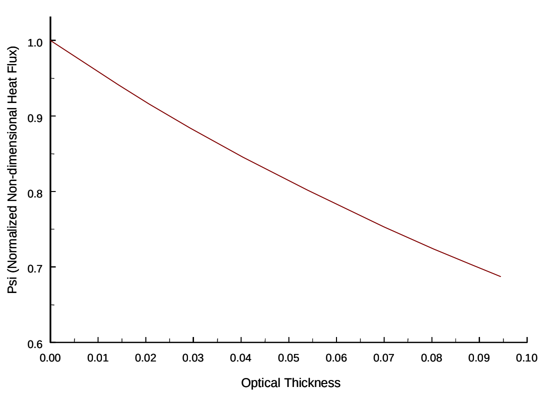

Figure 12. Optical Thickness vs. Relative Humidity.

Returning to the nine simulations illustrated in Figure 11, the largest optical thickness was about 0.095, with 100% relative humidity. This verifies the validity of the optically thin medium assumption for the simulations.

Leckner's functional expression of vapor emissivity was used to the absorption coefficients for each of the nine case study scenarios. Recall that Leckner's expression has a maximum error of less than ±5% to evaluate the emissivity for vapor temperatures higher than 100°C. The simulations utilized medium temperatures of 280 K, 290 K, and 300K that are 7°C, 17°C, and 27°C, respectively. Thus, the results may contain errors that are greater than ±5%. Even taking this possible error into account during the simulations, a noticeable effect of the absorption of radiative energy by the moist air was evident.

The conclusion from this section is that, under very humid conditions, it is important to include the impact of air moisture content on radiative transport.

4.0 Thermal Comfort and Radiant Heat Transfer

ASHRAE Standard 55 (1992) defines thermal comfort as "the condition of mind that expresses satisfaction with the thermal environment." The thermal comfort variables are: 1) activity level, 2) clothing insulation value, 3) air velocity, 4) humidity, 5) air temperature, and 6) mean radiant temperature (Fanger, 1967). For most design situations, the activity level and clothing value are determined by room usage, while air velocity and humidity depend on the thermal distribution system for the entire building. In an individual room, the air temperature and mean radiant temperature are the only two variables the design engineer may control.

Most thermal distribution systems are designed to maintain a baseline air temperature. Since radiant energy does not directly heat air, the air temperature does not measure the radiant energy exchange in a room. Rather, another variable is used. The mean radiant temperature (MRT) indicates the radiant energy exchange in a room, and is defined as "the uniform surface temperature of an imaginary black enclosure in which the radiation from the occupant equals the radiant heat transfer in the actual non-

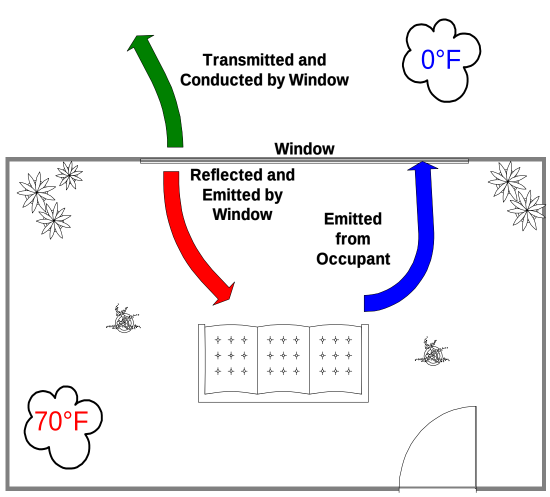

Figure 13: Non-Uniform Radiant Field.

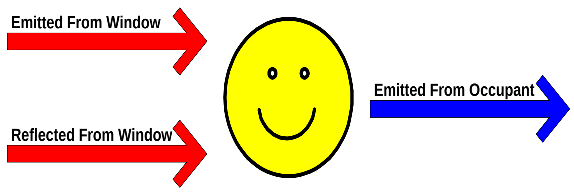

Figure 14: Radiative Energy Exchange Between a Window and an Occupant.

uniform enclosure" (Fanger, 1967). In a room where all the surfaces and air are at the same temperature, the mean radiant and air temperature are equal. As the difference between the surface temperatures and air temperature increases, the difference between the mean radiant and air temperature increases.

A typical example of a non-uniform radiant field, shown in Figure 13, is a room with a large window. The large thick arrows show the energy exchange for an occupant seated on the sofa. The radiation emitted from the occupant toward the window is caused by one or more of: 1) absorption by the window surface; 2) transmission to the outside environment; and/or 3) reflection back into the room.

Energy absorbed by the window surface can be conducted to the outside environment or emitted back into the room at the window surface temperature. The radiant energy exchange between the window and the occupant is shown in Figure 14. If the radiant energy emitted and reflected from the window to the occupant on the left side is less than the radiant energy emitted from the occupant to the window on the right side, then the occupant will feel chilled and be thermally uncomfortable. The mean radiant temperature will be less than the air temperature. To make the occupant thermally comfortable, an in-space convective heater or radiant heater could supplement the current thermal distribution system to offset the occupant heat loss and supply local thermal comfort.

This example shows that air temperature alone is not a good thermal comfort indicator. Instead Fanger (1967) suggests using the operative temperature (T_{op}) to measure local thermal comfort. The operative temperature is approximately the average of the air temperature and the mean radiant temperature and is more indicative of the temperature the occupant feels.

4.1 Mean Radiant and Operative Temperature

The mean radiant temperature is defined as "the uniform surface temperature of an imaginary black enclosure in which the radiation from the occupant equals the radiant heat transfer in the actual non-uniform enclosure" (Fanger, 1967; ASHRAE, 1992). The net radiation on a person is described as:

$$Q = \int I(\Omega) A_p(\Omega) d\Omega \tag{3.1}$$

This equation is a continuous summation over all the directions represented by the solid angle Ω (Siegel and Howell, 1981; Modest, 1993). The intensity and projected area in the direction Ω are represented by $I(\Omega)$ and $A_p(\Omega)$, respectively. Using the discrete ordinates method, the net radiation is calculated using a discrete approximation to the continuous form (equation (3.1)) by:

$$Q \cong I^j A_p^j w^j \tag{3.2}$$

The variable I^j is the intensity coming from a given discrete direction, w^j is the quadrature weighting function for that direction, A_p^j is the projected area in the given direction. The projected area from a given direction is given in the *ASHRAE HVAC Systems and Equipment Handbook* (1996). The general equation is:

$$A_p^j = f_p^j f_{eff} A_D \tag{3.3}$$

where f_p^j is the projected area factor in a given direction. Charts of these factors for sitting and standing people are given in Fanger (1967) and ASHRAE (1996). The effective radiation area of a person, f_{eff}, equals 0.73 for a standing person (ASHRAE, 1996). The DuBois area, A_D, is estimated from a person's height and mass. For an average person, A_D equals 1.821 m^2 (ASHRAE, 1996).

The net radiation from a black body enclosure is:

$$Q_{black} = A_{eff} \sigma T_{MRT}^4 \tag{3.4}$$

where:

$$A_{eff} = f_{eff} A_D \tag{3.5}$$

According to the definition of mean radiant temperature, equations (3.3) and (3.4) are equal. Solving for T_{MRT} results in:

$$T_{MRT} = \left(\frac{\sum_j I^i A_p^j w^j}{f_{eff} A_D \sigma} \right)^{\frac{1}{4}} \tag{3.6}$$

This equation provides an alternate approach to calculating the T_{MRT} as specified in the *ASHRAE Handbook of Fundamentals* (1993). Using the localized radiant intensity field should be more accurate than using radiosities from room surfaces. Furthermore, this approach is easily incorporated into BCAP methodology since the intensity field is calculated throughout the room. The operative temperature, T_{op}, can be calculated as the average of T_{MRT} and T_{air} (Fanger, 1967; ASHRAE, 1995). In the BCAP methodology, the T_{MRT}, the T_{air}, and the T_{op} at user-defined locations are calculated and stored in a file. In addition, the average T_{MRT} for the entire room is calculated and printed into room summary information.

4.2 Thermal Distribution Systems

Gan and Croome (1994) reported that almost 40% of the world's nonrenewable energy is used to achieve thermal comfort in buildings. Thermal distribution systems can use one or both of the two modes of heat transfer, convection and radiation, to deliver thermal comfort to an occupant. Figure 15 illustrates the difference in heating modes. The forced-air system on the left primarily uses convection to deliver the heat energy to the occupant by heating the air first. Then the air heats the occupant. With a radiant system, which

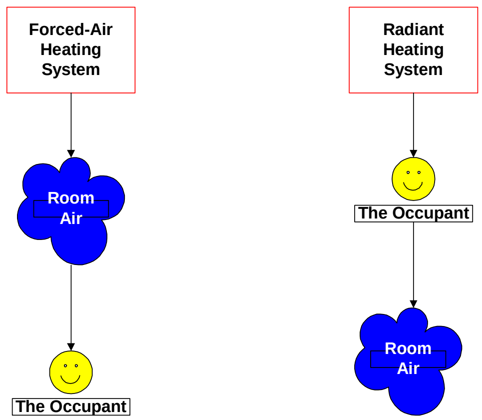

Figure 15: Thermal Comfort Delivery.

appears on the right, the occupant is heated first. Then the occupant and the other room surfaces heat the surrounding air. To mathematically model a heating system and predict the thermal comfort of an occupant, the relative amounts of energy transferred by each mode called the radiative/convective split must be known.

This section briefly describes three major types of heating systems: 1) in-space convective heating systems; 2) radiant heating systems; and 3) hybrid systems. In addition, a literature review on the radiative/convective split for specific heaters is summarized.

4.2.1 In-Space Convective Heating Systems

In-space heaters convert fuel to heat for a specific space that is to be heated (ASHRAE, 1996). Examples of in-space heaters are wall and floor furnaces, baseboard heaters, cord-connected portable heaters, stoves, and fireplaces. The fuel may be gas, oil, electricity, or a solid fuel. In-space heaters provide thermal comfort to a room by a combination of forced and natural convection and radiation. Chapter 29 in the *1996 ASHRAE Systems and Equipment Handbook* provides detailed information about in-space heaters including descriptions, minimum annual fuel utilization efficiencies, and control information.

4.2.2 Radiant Heating Systems

Radiant heating systems transmit energy to the occupant and objects in a specific space through electromagnetic waves. Note that thermal radiation does not directly heat the air. Gases such as nitrogen, and therefore air, are relatively transparent to thermal radiation except at very high temperatures exceeding 2,000 K (3,140°F) (Özisik, 1977). With a radiant heating system in a typical room, air will not absorb or emit radiant energy. Examples of radiant heaters are embedded piping in ceilings or floors, electric ceiling or wall panels, and electric heating cable in ceilings or floors (ASHRAE, 1995). Chapter 49 in the *ASHRAE HVAC Applications Handbook* (1995) and Chapter 15 of the *ASHRAE HVAC Systems and Equipment Handbook* (1996) provide more information on radiant heating including types of radiant heaters and design considerations.

4.2.3 Hybrid Systems

Hybrid systems combine convective and radiant heaters. The convective system is used to maintain a baseline air temperature. Usually, the convective system is purposefully undersized with the intent that the radiant heater will provide the difference. The radiant heater provides localized thermal comfort to occupied spaces. The goal of a hybrid system is to eliminate severe temperature gradients in a room. Currently, the ASHRAE handbook series does not contain a specific chapter on this type of heating system.

4.3 Heater Output Distribution Literature Search

To accurately model the thermal comfort distribution in a room, the relative portions of heat contributed by convective and radiant heat transfer must be known. Although some manufactures provide this data, a documented source with carefully collected and analyzed results would provide the most reliable information.

To this end, an exhaustive search for the radiative/convective split for fireplaces, stoves, wall and floor furnaces, baseboard heaters, portable cord-connected heaters, and radiant panels was conducted. The search included extensive use of the Engineering Information Village's Compendex journal database and the use of DIALOG for seven relevant databases with records dating back to 1969. While a a large number of articles were found and reviewed as a result of these searches, no documentation on the radiative/convective split was found.

4.4 Thermal Comfort Simulation

The most economical way to predict thermal comfort conditions in a room is to mathematically model the room using a computer to handle the complex and tedious calculations. Jones and Chapman first developed the BCAP methodology, which provides a set of mathematical equations describing convective and radiative heat transfer, in 1994 under ASHRAE RP-657. Chapman and Zhang (1995, 1996) and Chapman et al. (1997) have demonstrated this methodology. This section discusses the robust mathematical equations used by the methodology, the output the user obtains, and previous validation of the methodology.

To accurately model a room, general equations need to rigorously describe the room and be solved with accurate methods. In a room, the three methods of heat transfer, conduction, convection, and radiation, are present. While conduction and convection are relatively simple to model, radiative heat transfer is more complex to characterize. This section explains the energy balances for the mathematical description of a room.

The governing heat transfer equations for the room air and for each wall surface within a room as presented by Jones and Chapman (1994) and Chapman and Zhang (1995) are:

$$\sum_{i=1}^{N}(h_i A_i (T_{air} - T_i) + \dot{m}_{if}\int_{T_o}^{T_{air}} c_p(T)dT + \dot{Q}_{h,c} = \frac{\partial E_{air}}{\partial t} \tag{3.7}$$

$$\frac{(T_o - T_i)}{R_{th}} + h_i(T_{air} - T_i) + \left\{\alpha_i \int_{\bar{n}\bullet\Omega<0} |\mathbf{n}\bullet\Omega| I(\Omega)d\Omega' - \varepsilon_i \sigma T_i^4\right\} + \dot{Q}_{rad,panel} = \frac{\partial E_i}{\partial t} \tag{3.8}$$

Equation (3.7) describes the room air energy balance. The first term on the left is the convective losses to the wall surfaces. The second term is the infiltration rate where T_o is the temperature of the infiltrating air. The last term is the convective heat transfer provided by the heating system. The right side of the equation represents the time rate change in energy of the air. At steady-state conditions, this term is zero.

Equation (3.8) describes the energy balance for a wall surface at T_i. The first term is the conduction through the wall, where T_o is the outside air temperature and R_{th} represents the thermal resistance of the wall and outer convective boundary layer. The second term is the convective flux between the room air and the wall surface. The third term is the net radiant heat flux from incident energy and emissive energy. The fourth term is the net radiant heat flux from the heating source. The term on the right of the equation represents the change in energy of the surface. Again at steady-state conditions, this term is zero.

5.0 Modeling Features

The problem at hand is to enhance the BCAP methodology in order to analyze the impact of obstacles within the enclosed space on thermal comfort. While this may at first seem a straight-forward task, the internal boundaries of the room offer a unique challenge and must be incorporated in an appropriate manner. Figure 15 illustrates a room with a radiant panel heater positioned on the ceiling. The room also includes a partition. The partition impacts the radiation field, and hence the radiation calculations, in two ways. First, the partition shades the area to the right of it from the radiant heater. This area of the room can no longer "see" the radiant panel. The second impact is that the partition itself becomes a re-radiating boundary inside the enclosed space. To complicate the issue even more, the temperature of the partition may be different on one side than it is on the other. Consequently, heat transfer through the partition must be considered.

5.1 Conservation of Energy Equation

The conservation of energy equation is the fundamental relationship that results in the temperature distribution throughout the room. This equation, written on a control volume basis, is (refer to the upper left panel in Figure 16):

$$0 = \dot{q}_{E \to P} + \dot{q}_{W \to P} + \dot{q}_{N \to P} + \dot{q}_{S \to P} + \left(G - E\right) + \dot{q}_{in} \tag{4.1}$$

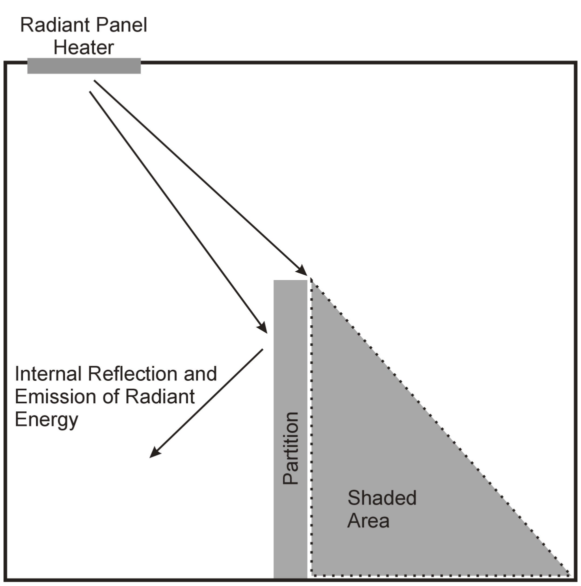

Figure 15: Impact of Shading.

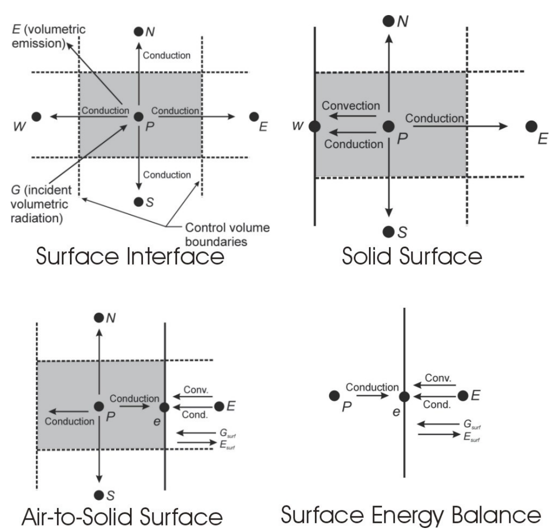

Figure 16: Control Volumes for Interior Surfaces.

This equation includes conduction heat transfer from the center point node P to the surrounding nodes, the rate that radiant energy is incident on the control volume (G), the rate that radiant energy leaves the control volume (E), and any internal heat generation ($\dot{q}_{in}$). The term $(G-E)$ is determined by solving the RTE. Internal heat generation is present if the control volume represents a heater or cooler. Heat conduction is determined by:

$$\dot{q}_{E\rightarrow P} = \frac{k}{\delta}\left(T_E - T_P\right) \tag{4.2}$$

where k is the thermal conductivity and δ is the distance between nodes E and P.

Equation (4.1) works well for all control volumes within the room except for those that are adjacent to a solid surface. The upper right panel in Figure 16 illustrates the modifications that are necessary to incorporate the effects of the solid surface. The most notable difference is that energy is transferred between the control volume and the solid surface by convection in addition to conduction. The more general form of the equation is:

$$\begin{aligned} 0 &= \dot{q}_{E\rightarrow P} + h_w\left(T_w - T_P\right) + \dot{q}_{W\rightarrow P} \\ &+ \dot{q}_{N\rightarrow P} + \dot{q}_{S\rightarrow P} + \left(G-E\right) + \dot{q}_{in} \end{aligned} \tag{4.3}$$

If the solution is independent of wavelength, the surface radiation terms are calculated by:

$$E_{surf} = \varepsilon_{surf}\sigma T_{surf}^4 \tag{4.4}$$

$$G_{surf} = \varepsilon_{surf}\int_{\text{Incoming}} I\left(\Omega\right)\mu d\Omega \approx \varepsilon_{surf}\sum_{\text{Incoming}} I^j w^j \mu^j \tag{4.5}$$

If the solution depends on wavelength i.e., some or all of the radiation properties are wavelength dependent, then calculation of the surface radiation heat transfer terms is somewhat more complex.

Finally, additional complexity is added if the boundary is an internal boundary. The lower left panel in Figure 16 illustrates this case. Focusing again on point P, the boundary of the control volume now includes convection and conduction heat transfer, plus the incident radiation G_{surf} and the emitted radiation E_{surf}. The energy balance on the control volume is:

$$0 = \dot{q}_{E\to e} + h_e \left(T_E - T_e\right) + \dot{q}_{W\to P} + \dot{q}_{N\to P} + \dot{q}_{S\to P} + \left(G_{surf} - E_{surf}\right) + \dot{q}_{in} \qquad (4.6)$$

The only remaining task is to calculate the boundary surface temperatures. This is accomplished by conducting a surface energy balance as shown by the lower right panel in Figure 16. The surface energy balance provides closure to the conservation of energy equation and is written for each surface in the room. The surface energy balance is:

$$\dot{q}_{cond,P\to e} = h_e \left(T_E - T_e\right) + \dot{q}_{cond,E\to e} + G_{surf} - E_{surf} \qquad (4.7)$$

Collectively with the RTE, equations (4.3) through (4.7) are solved to determine the temperature and radiation distribution within a room, with or without partitions.

5.2 Solving the Conservation and Radiation Equations

To implement these equations, the room is divided into control volumes as shown in Figure 17. The radiant panel heater, the room, and the partition are separated into small control volumes. Equations (4.3) and (4.6) are solved for each control volume in the room, and equation (4.7) is solved for each surface in the room. The radiation equations are solved in the exact same way as described by Jones and Chapman (1994) and Chapman and DeGreef (1997). The only additional calculation is that the radiant fluxes must be calculated at the internal surfaces.

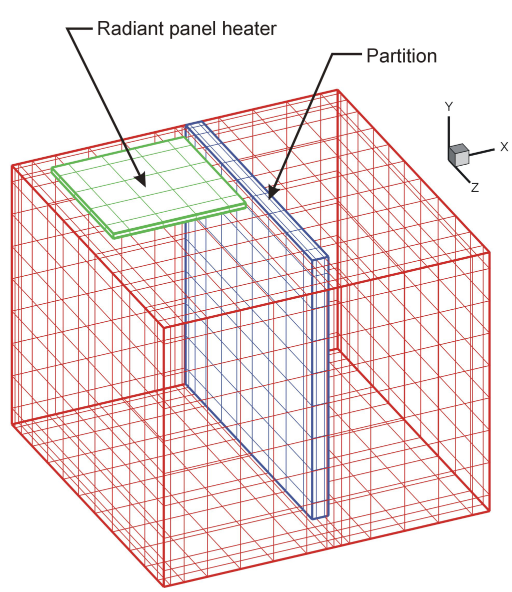

Figure 17: Internal Surface.

6.0 Demonstration Cases

Four examples demonstrate various applications of high temperature radiant heaters. The heaters used in the demonstration cases range from indirect tube heaters that could approach temperatures of 2,000°F to smaller spot-type electrical heaters used to heat localized work locations. In each case, contour plots show the distribution of the dry-bulb temperature and the operative temperature throughout the room. The contour plots show not only areas of thermal comfort, but also asymmetry and air temperature stratification.

6.1 High Temperature Tube Heater with Reflectors

This case is for a large space that is heated with two and four indirect tube heaters. The space is 80 ft wide and 125 ft long with a ceiling 16 ft above the floor to allow for operation of a 10-ton overhead crane. The space is located over a heated sub-flooring system that is maintained at 50°F. The external temperatures on all sides of the conditioned space is 0°F. The sub-flooring system and the external temperatures are the same for each of the four demonstration cases. The goal of this demonstration case is to establish an average operative temperature of 70°F at a location three feet above the floor. The wall *R*-values are 11 and the ceiling *R*-value is 30. The building also contains a row of windows on the north wall. The windows are 2 ft high and have an *R*-value of 2.

One simulation was run with two heaters, and results are shown in Figures 18 and 19. A second simulation was completed with four heaters and Figures 20 and 21 show these temperature distributions. Specifically, Figures 18 and 20 show the plane that is located 3 ft above the floor, while Figures 19 and 21 display the operative temperature contour across

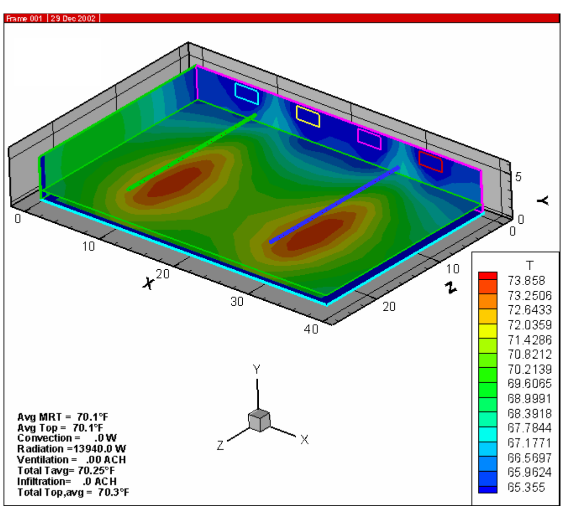

Figure 18: Operative Temperature 3 ft above the Floor with Two Tube Heaters.

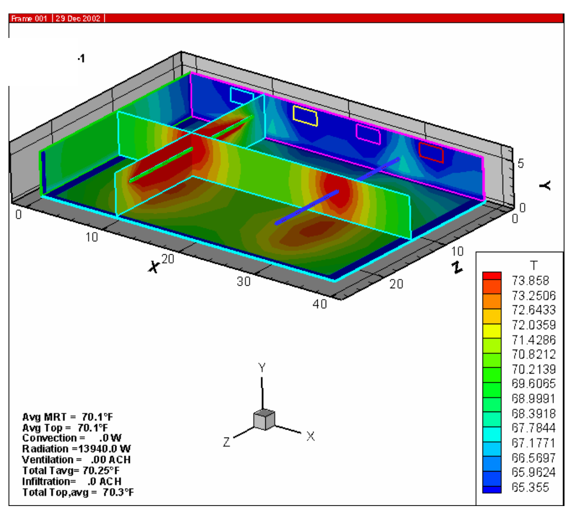

Figure 19: Operative Temperature in the Room with Two Tube Heaters.

the heater in the X and Z directions.

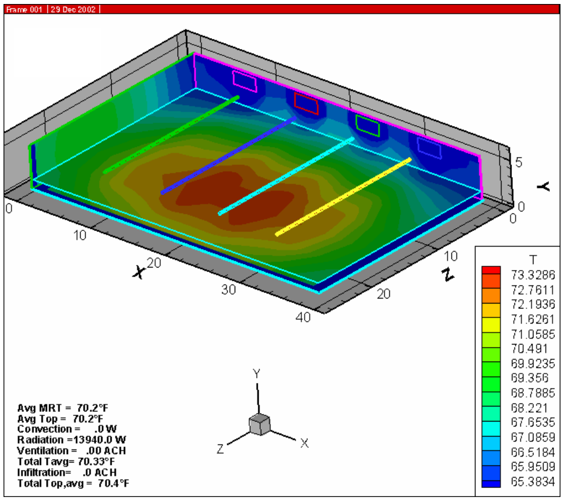

Figure 20: Operative Temperature 3 ft above the Floor with Four Tube Heaters.

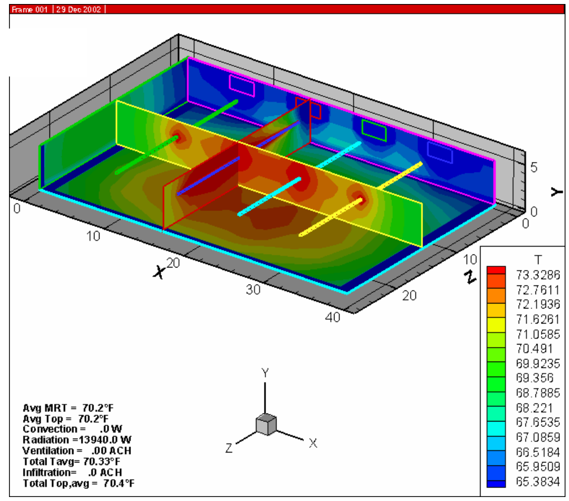

Figure 19: Operative Temperature in the Room with Four Tube Heaters.

In both simulations, an iterative method was used to estimate the total heat output from the heaters to maintain the average T_{op} at 70°F. The result is that approximately the same amount of heat, 13,940 watts, is needed in both scenarios.

Two observations can be drawn from these four figures. First, the surface temperature of the back wall clearly shows the location of the window (Figures 18 and 20). As expected, the surface temperature of the window is lower than the surface temperature of the rest of the back wall. Similarly, the contours in the x-direction in Figures 19 and 21 show the influence of the windows so that the temperatures near the windows are lower than the farther locations.

Another observation is that the temperatures near the heaters are obviously higher than the margin areas. Comparing Figure 18 and 19 to Figure 20 and 21 leads to the conclusion that the heaters' location and number significantly impact the room operative temperature distribution. Figures 18 and 20 with only two heaters show a larger operative temperature gradient especially in the margin areas than that of Figures 19 and 21 with four heaters. Therefore, the T_{op} field may be made more uniform by distributing the total heat power through the use of more heaters.

6.2 Factory Spot Heating for Thermal Comfort

This case is similar to the first case with the exception that only specific locations need to be thermally comfortable. For this application, high temperature electrical heaters are used to focus energy on the occupied locations. There are six heaters spaced uniformly within the building structure. This case compares the results of the heaters positioned two feet from the ceiling to the case where the heaters are positioned six feet from the ceiling. The sub-flooring system and the external temperatures are the same as the previous case.

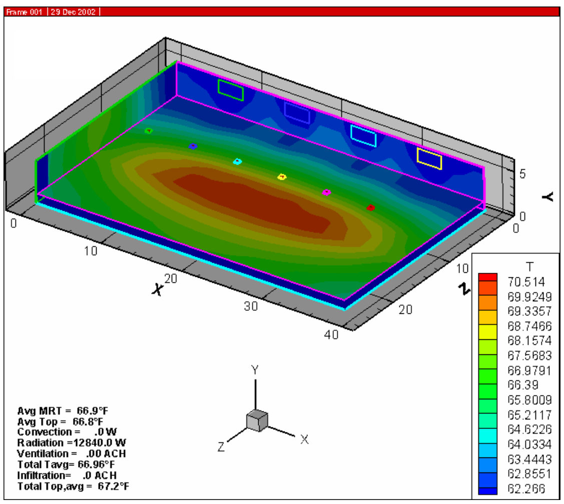

Figure 22: Operative Temperature 3ft above the Floor with Six Tube Heaters Located 2 ft from the Ceiling.

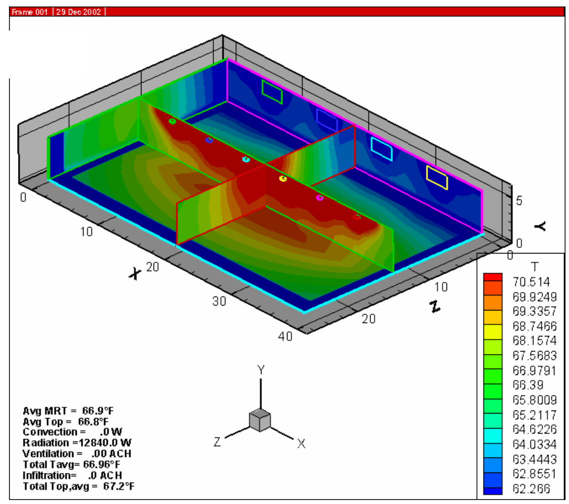

Figure 23: Operative Temperature on the Room with Six Tube Heaters Located 2 ft from the Ceiling.

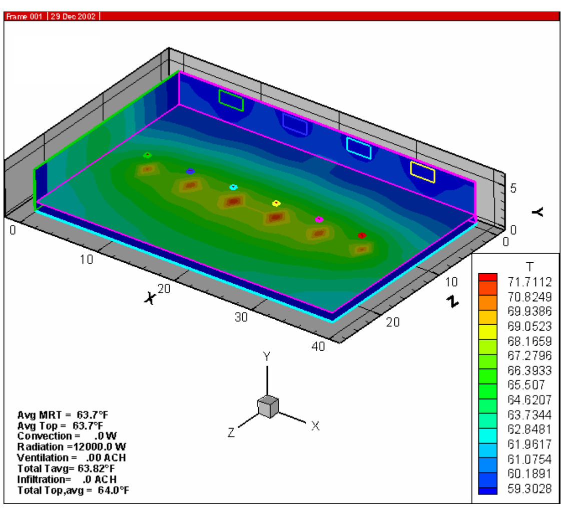

Figure 24: Operative Temperature 3 ft above the Floor with Six Tube Heaters Located 8 ft from the Ceiling.

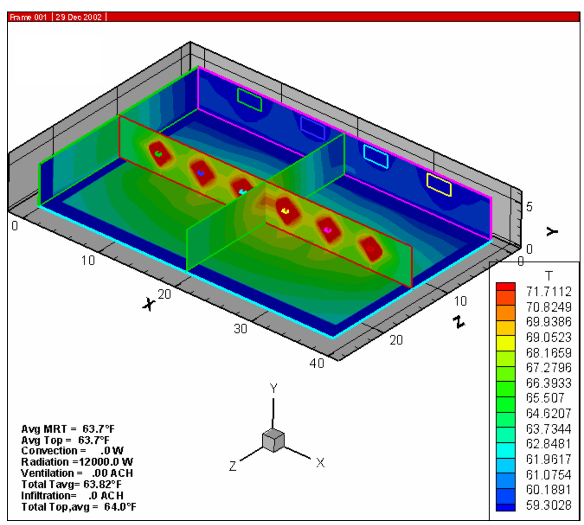

Figure 25: Operative Temperature in the Room with Six Tube Heaters Located 8 ft from the Ceiling.

Figures 22 through 25 illustrate the operative temperature distribution throughout the room in several different planes where the six heaters are located different distances from the ceiling. To determine the required thermal comfort in the occupied locations, different heater outputs are applied in the two cases. Heaters that are located higher above the floor require more heating power to create the thermally comfortable spaces. Additionally, heaters that are located closer to the work location allows for their heat output to be used more efficiently and thus less heat power is required.

6.3 Occupied Space with High Ceilings

The floor footprint for this case is 40 ft by 40 ft with a 12 ft ceiling. The structure contains no windows. The simulation demonstrates the limits of a heater to provide uniform occupant thermal comfort inside the room. Just one tube heater located 2 ft below the ceiling is used in this simulation, which is the same as case 6.1. While the heater power is 3,350 watts, the surface temperature of the heater is limited to 900°F so as to prevent illumination within the room. This case represents new construction, and as such the wall *R*-values are 11 and sub-flooring is maintained at 30°F.

The results shown in Figures 26 and 27 show that if the surface area of the heater is very small, then the highest temperature of the heater will become higher than 900°F. Therefore,

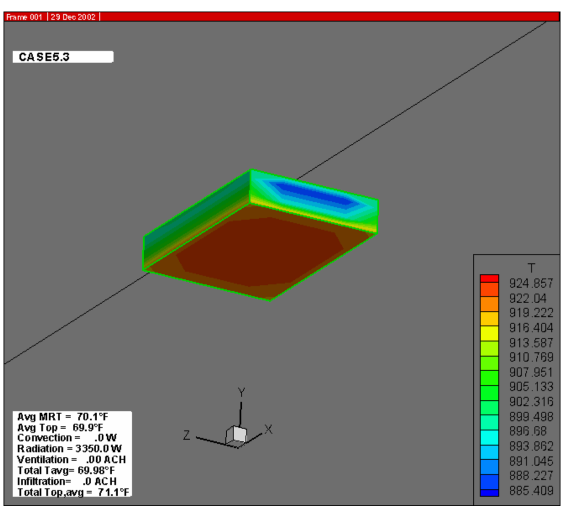

Figure 26: Surface Temperature Distribution with the Heater Located 2 ft from the Ceiling.

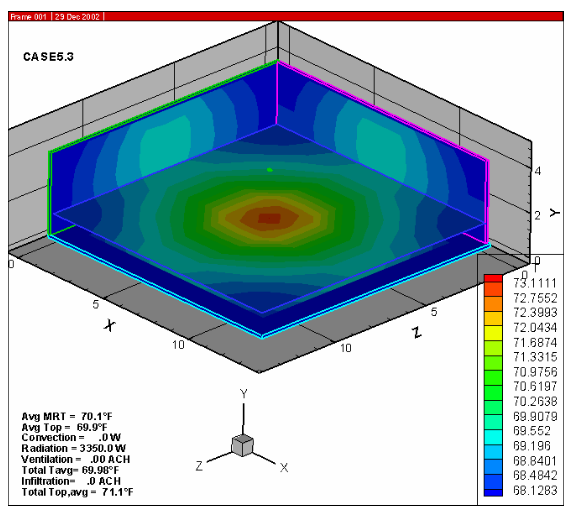

Figure 27: Operative Temperature Distribution at 3 ft above the Floor and a Heaters Located 2 ft from the Ceiling.

to prevent illumination within the room it is required that the surface area of the heater cannot be very small and its heat power cannot be very high.

6.4 Warehouse for Thermal Comfort and Freeze Protection

This demonstration case shows the high temperature heating requirements for a warehouse that is 1,000 ft by 500 ft with a 20 ft ceiling. The goal is to maintain all areas of the warehouse at a dry-bulb temperature of at least 35°F to provide freeze protection, and the work location at an operative temperature of 60°F. The work location is open to the rest of the warehouse, and is located at one end of the warehouse. The demonstration shows the effective use of indirect tube heaters and high temperature electric heaters to create a hybrid heating system.

Figures 28 and 29 illustrate that the requirements of an operative temperature of 60°F and a dry-bulb temperature of 35°F in the whole warehouse can be achieved by applying a high-temperature electric heater near the work location. Figure 29 focuses only on the local operative temperature distribution within the relatively small work space.

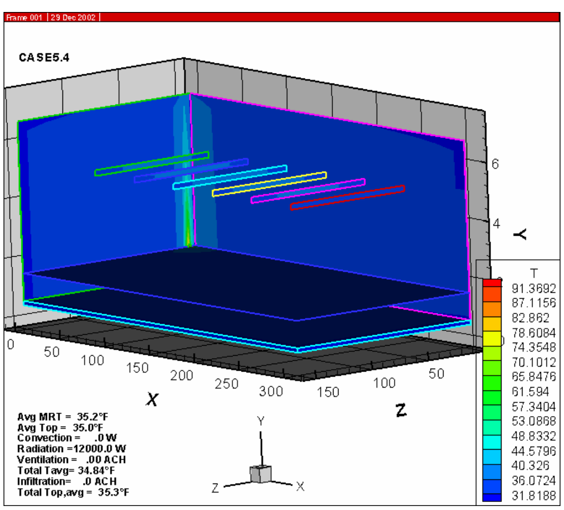

Figure 28: Operative Temperature Distribution at 3 ft above the Floor with Combined Heaters.

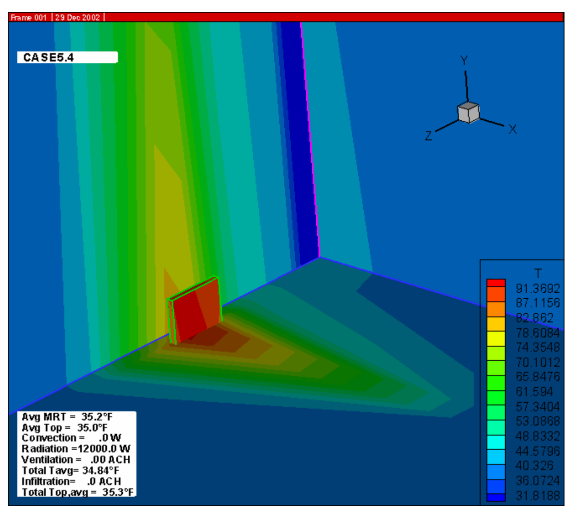

Figure 29: Operative Temperature Distribution in the Work Location using Combined Heaters.

7.0 Conclusions

High temperature radiant heaters are used to provide thermal comfort in a variety of applications, such as materials processing, aircraft hangars or warehouses. The most attractive advantage of a radiant heater is its capability to supply heat to the occupants without having to use the surrounding air as the medium of energy transfer. For spaces that have a high rate of air change per hour, or where the entire air volume does not need to be conditioned, high temperature radiant heating will be more efficient if for no other reason than only the occupied space needs to be conditioned.

Based on the principle of energy transfer, the conservation of energy equation and the radiation equations are constructed and solved by using the discrete ordinate model. Four demonstration cases are displayed to illustrate the main factors to the temperature distribution inside the room. Several distinctive conclusions are drawn from these cases.

1. The most popular heaters used in high-temperature radiant heat transfer are two types: tube heater and high-temperature electrical heater. These heaters can be combined to maintain the overall freeze protection and the thermal comfort in special locations.

2. The location and number of the heaters can be the most important factor to the temperature and operative temperature distribution inside the room. For example, by repositioning the heaters or distributing heater power to more heaters, a more uniform T_{op} field can be achieved. To provide the thermal comfort in special areas it is possible to locate the radiant heater closer to the work location.

3. Although the definition of the high-temperature heater is one whose surface is greater than 300°F or may be as high as 1800°F, the surface temperature of a heater should be maintained lower than 900°F if illumination is an issue.

4. In large open spaces, such as a warehouse or aircraft hangars where freeze protection and special thermal comfort in some spots is required, a combination of tube heaters and panel electrical heaters can successfully be used to meet the desired requirements.

8.0 References

American Society of Heating, Refrigerating and Air Conditioning Engineers, Inc. (ASHRAE), 1992. ASHRAE Standard 55-1992. "Thermal Environmental Conditions on Human Occupancy," Atlanta, Georgia.

American Society of Heating, Refrigerating and Air Conditioning Engineers, Inc. (ASHRAE), 1993. *ASHRAE Handbook of Fundamentals*, Atlanta, Georgia.

American Society of Heating, Refrigerating and Air Conditioning Engineers, Inc. (ASHRAE), 1995. *ASHRAE HVAC Applications Handbook*, Atlanta, Georgia.

American Society of Heating, Refrigerating and Air Conditioning Engineers, Inc. (ASHRAE), 1996. *ASHRAE HVAC Systems and Equipment Handbook*, Atlanta, Georgia.

Brewster, M.Q., 1992. *Thermal Radiative Transfer & Properties*, John Wiley and Sons: New York.

Carlson, B.G. and Lathrop, K.D., 1963. *Transport Theory—The Method of Discrete-Ordinates in Computing Methods in Reactor Physics*, eds. Grenspan, Keller and Okrent, Gordon and Breach: New York.

Chapman, K.S. and DeGreef, J.M., 1997. "Design Factor Development to Obtain Thermal Comfort with Combined Radiant and Convective In-Space Heating and Cooling Systems," Final Report of ASHRAE Research Project RP-907, ASHRAE: Atlanta, Georgia.

Chapman, K.S., Ramadhyani, S., and Viskanta, R., 1992, "Modeling and Parametric Studies of Heat Transfer in a Direct-Fired Furnace with Impinging Jets," presented at the 1992 ASME Winter Annual Meeting, Anaheim, CA.

Chapman, K.S. and Zhang, P., 1995. "Radiant Heat Exchange Calculations in Radiantly Heated and Cooled Enclosures," *ASHRAE Transactions* 101 (I).

Chapman, K.S. and Zhang, P., 1996, "Energy Transfer Simulation for Radiantly Heated and Cooled Enclosures," *ASHRAE Transactions* 102 (I).

Chapman, K.S., DeGreef, J.M., and Watson, R. D., 1997. "Thermal Comfort Analysis Using BCAP for Retrofitting a Radiantly Heated Residence," *ASHRAE Transactions* 103 (I).

Fanger, P., 1967. "Calculation of Thermal Comfort: Introduction of a Basic Comfort Equation," *ASHRAE Transactions* 73(II):1-20.

Fiveland,W.A., 1984, "Discrete-Ordinates Solutions of the Radiative Transport Equation for Rectangular Enclosures," *J. Heat Transfer*, 106, pp. 699-706.

Fiveland, W.A. and Jamaluddin, A.S., 1989, "Three Dimensional Spectral Radiative Heat Transfer Solutions by the Discrete-Ordinates Method," ASME Heat Transfer Conference Proceedings, Heat Transfer Phenomena in Radiation, Combustion, and Fires, ASME, New York, HTD-Vol. 106, pp. 43-48.

Fiveland, W. A., 1988. "Three Dimensional Radiative Heat-Transfer Solutions by the Discrete-Ordinates Method," *Journal of Thermophysics Heat Transfer*, 2:4, pp. 309-316.

Gan, G. and Croome, D. J., 1994, "Thermal Comfort Models Based on Field Measurements," ASHRAE Transaction 100 (I).

Harder, R., Ramadhyani, S., and Viskanta, R., 1987. "Gas-Fired Radiant Tubes: A Review of Literature," Topical Report, GRI-87/0343, Gas Research Institute: Chicago, Illinois.

Hottel, H.C., 1954, "Radiant-Heat Transmission," in W.H. McAdams, Ed., *Heat Transmission*, 3rd edition, McGraw-Hill, New York.

Hottel, H.C. and Sarofim, A.F., 1967. *Radiative Transfer*, McGraw-Hill: New York.

Jones, B. and Chapman, K.S., 1994. "Simplified Method to Factor Mean Radiant Temperature (MRT) into Building and HVAC System Design,"Final Report of ASHRAE Research Project RP-657, ASHRAE: Atlanta, Georgia.

Leckner, B., 1972. "Spectral and Total Emissivity of Water Vapor and Carbon Dioxide," *Combustion and Flame*, 19, pp. 33-48.

Modest, M.F., 1993. *Radiative Heat Transfer*, McGraw-Hill: New York.

Moran, M.J. and Shapiro, H.N., 1992. *Fundamentals of Engineering Thermodynamics*, John Wiley and Sons: New York.

Özişik, M. N., 1977. *Basic Heat Transfer*, McGraw-Hill: New York.

Patankar, S. V., 1980, *Numerical Heat Transfer and Fluid Flow*, McGraw-Hill, New York.

Sanchez, A., and Smith, T.F., 1992, "Surface Radiation Exchange for Two-Dimensional Rectangular Enclosures Using the Discrete-Ordinates Method," J. Heat Transfer, 114, pp. 465-472.

Severens, P.F.J., Bouma, P.H., van de Van, C.J.H., de Goey, L.P.H., and van der Drift, A., 1995. "Modeling of Twofold Flame Behavior of Ceramic Foam Surface Burners," *Journal of Energy Resources Technology*.

Siegel, R. and Howell, J.R., 1981. *Thermal Radiation Heat Transfer*, McGraw-Hill: New York.

Solaronics, Inc., 1994a. *Spot and Area Heating: Design Guide*, Rochester, Michigan.

Solaronics, Inc., 1994b. *Total Building Heating Design Guide: Infra-red Heaters*, Rochester, Michigan.

Truelove, J.S., 1987. "Discrete-Ordinates Solutions of the Radiative Transport Equation," *Journal of Heat Transfer*, 109, pp. 1048-1051.

Truelove, J.S., 1988. "Three-Dimensional Radiation in Absorbing-Emitting Media," *Journal of Quantitative Spectrosc. Radiat. Transfer*, 39:1, pp. 27-31.

Viskanta, R. and Mengüc, M.P., 1987. "Radiation Heat Transfer in Combustion Systems," *Prog. Energy Combustion Science*, 13.

Viskanta, R. and Ramadhyani, S., 1988. "Radiation Heat Transfer in Directly Fired Natural Gas Furnaces: A Review of Literature," Topical Report, GRI-88/0154, Gas Research Institute: Chicago, Illinois.